ÉCOLE POLYTECHNIQUE FÉDÉRALE DE LAUSANNE

MATHICSE

Mathematics Institute of Computational Science and Engineering

School of Basic Sciences - Section of Mathematics

MATHICSE Technical Report

Nr. 07.2015

March 2015

Isogeometric analysis of high order partial differential equations on surfaces

Andrea Bartezzaghi, Luca Dedè, Alfio Quarteroni

http://mathicse.epfl.ch

Phone: +41 21 69 37648

Address:
EPFL - SB - MATHICSE (Bâtiment MA)
Station 8 - CH-1015 - Lausanne - Switzerland

Fax: +41 21 69 32545

Isogeometric Analysis of High Order Partial Differential Equations on Surfaces

Andrea Bartezzaghi [1,*], Luca Dedè [1], and Alfio Quarteroni [1,2]

[1] CMCS – Chair of Modeling and Scientific Computing
MATHICSE – Mathematics Institute of Computational Science and Engineering
EPFL – École Polytechnique Fédérale de Lausanne
Station 8, Lausanne, CH–1015, Switzerland

[2] MOX – Modeling and Scientific Computing
Department of Mathematics
Politecnico di Milano
Piazza L. da Vinci 32, Milano, 20133, Italy (on leave)

March 16, 2015

Abstract

We consider the numerical approximation of high order Partial Differential Equations (PDEs) defined on surfaces in the three dimensional space, with particular emphasis on closed surfaces. We consider computational domains that can be represented by B-splines or NURBS, as for example the sphere, and we spatially discretize the PDEs by means of NURBS-based Isogeometric Analysis in the framework of the standard Galerkin method. We numerically solve benchmark Laplace-Beltrami problems of the fourth and sixth order, as well as the corresponding eigenvalue problems, with the goal of analyzing the role of the continuity of the NURBS basis functions on closed surfaces. In this respect, we show that the use of globally high order continuous basis functions, as allowed by the construction of periodic NURBS, leads to the efficient solution of the high order PDEs. Finally, we consider the numerical solution of high order phase field problems on closed surfaces, namely the Cahn-Hilliard and crystal equations.

Key words. High order Partial Differential Equations; Surfaces; Isogeometric Analysis; Error estimation; Laplace-Beltrami operators; Phase field models.

*Corresponding author. E–mail: andrea.bartezzaghi@epfl.ch. Phone: +41 21 6930359. Fax: +41 21 6935510.

1 Introduction

In several mathematical models we face Partial Differential Equations (PDEs) defined on lower dimensional manifolds [4]. Examples can be found in Fluid Dynamics, Mechanics, Biology, Electromagnetism, image processing [7, 17, 35, 36], where three dimensional problems are represented on surfaces, for instance in the case of thin geometries, modeled as membranes, plates, or shells [41], depending on the structure of the original domain. This leads to define surface PDEs which often involve high order differential operators [7, 23].

Usually, the numerical solution of surface PDEs is tackled using the Finite Element Method (FEM) [33]. In this case, a challenge for obtaining an accurate numerical approximation is the construction of a suitable computational mesh, which still represents an approximation of the original surface. Indeed, generating a mesh of "good quality" is necessary to accurately represent the surface, but also to evaluate the differential operators which are associated to the geometrical properties of the manifold. In particular, this involves the evaluation of several geometrical quantities, as the normal and curvature of the surface. In this context, accurately representing such geometric information is important also for the approximation of the PDEs. Besides being time consuming, the process of mesh generation may require a large number of Degrees Of Freedom (DOFs) for the PDE approximation. In the FEM context, different approaches have been introduced aiming at controlling the approximation error induced by the discretization of the geometry; examples are the surface FEM [15, 16], or geometrically consistent Adaptive FEM [28, 29, 30]. Other approaches are based on modeling the surfaces as immersed in the 3D domain or treated implicitly, as e.g. for level set formulations [5, 17] or diffuse and resistive interface approaches [2, 35].

In alternative to the above mentioned methods, we propose in this paper the use of Isogeometric Analysis [11, 25] for the numerical approximation of high order PDEs defined on surfaces. This choice is mainly motivated by the ability of NURBS and B-splines to exactly represent several geometries of practical interest [31], especially in industrial applications. Isogeometric Analysis (IGA) is a discretization method for approximating PDEs based on the isogeometric paradigm, for which the same basis functions are used first for the geometrical description of the domain and then for the numerical approximation of the solution of the PDEs [11, 25]; in this respect, IGA was developed with the goal of filling the gap between Computer Aided Design (CAD) and FEM, by providing a unified representation of the geometrical design, the computational domain, and the approximation function spaces. One potential advantage of IGA is thus its ability to directly use the description of the geometry for the spatial discretization of the PDEs, without requiring the time-consuming process of generating a computational mesh, which often only represents an approximation of the geometry. Indeed, in IGA many geometries of practical interest can be represented exactly at the coarsest level of discretization, with refinement procedures not affecting the geometrical representation, but only enhancing the approximation properties of the finite dimensional spaces.

While IGA is nowadays adopted for several geometrical representations [3, 38], including T-splines [39], we focus in this paper on B-splines and NURBS surfaces [31] built as single patches; indeed, open and closed surfaces can be suitably defined by NURBS, as it is the case of the sphere. While the numerical approximation of second order PDEs on surfaces by IGA has been extensively analyzed in [13], in this paper we focus instead on high order PDEs. Indeed, in this respect, other than the geometric advantages, IGA allows the spatial approximation of PDEs of order $2m$, with $m \geq 1$, by using the standard Galerkin formulation, without invoking the mixed formulations required by the isoparametric FEM [24] with the standard Lagrange polynomial basis functions for $m \geq 2$. The possibility of using globally C^k-continuous NURBS basis functions, with $m-1 \leq k \leq p-1$ and p the polynomial degree, yields IGA finite dimensional spaces that are

subspaces of the trial and test Hilbert spaces H^m required for PDEs of order $2m$, with $m \geq 1$ [40]. In addition, periodic NURBS basis functions can be built on surfaces with the goal of obtaining globally high order continuous NURBS function spaces [27]. This in turn allows the construction of NURBS function spaces of the required regularity and thus the solution of high order PDEs defined on closed surfaces. In this paper we consider IGA approximations of elliptic PDEs with high order Laplace-Beltrami operators, specifically of fourth and sixth order. We study the convergence rate of the errors, for both PDEs on open and closed surfaces, and eigenvalue problems. Then, in order to show the efficiency and robustness of our approach, we solve phase field problems, namely the Cahn-Hilliard and phase field crystal equations on closed surfaces, both being high order, nonlinear, and time dependent PDEs.

This paper is organized as follows. In Section 2 we provide a quick introduction to the geometrical representation of surfaces by means of NURBS. The mathematical tools needed to define high order PDEs on surfaces are described in Section 3, together with the biharmonic and triharmonic Laplace-Beltrami problems and the corresponding eigenvalue problems. In Section 4 the spatial discretization by IGA is introduced, together with a discussion about the enforcement of global continuity of the basis functions on closed surfaces. Numerical results on benchmark problems are reported and discussed in Section 5. The high order phase field problems, and specifically the fourth order Cahn-Hilliard equation on the unit sphere and the sixth order phase field crystal equation on a torus, are solved in Section 6. Finally, conclusions follow.

2 NURBS: Surfaces and Function Spaces

In this section we recall the basic notions of NURBS geometries and basis functions, with particular emphasis on the representation of surfaces and construction of NURBS function spaces.

2.1 NURBS surfaces and basis functions

Given a parameter domain $\widehat{\Omega} \subset \mathbb{R}^2$ of finite and positive measure in the topology of $\mathbb{R}^2$ and a vector-valued independent variable $\boldsymbol{\xi} = (\xi_1, \xi_2) \in \mathbb{R}^2$ called *parametric coordinate*, let us consider the compact, connected, and oriented manifold $\Omega \subset \mathbb{R}^3$, defined by the geometrical mapping:

$$\mathbf{x} : \widehat{\Omega} \to \Omega \subset \mathbb{R}^3, \qquad \boldsymbol{\xi} \to \mathbf{x}(\boldsymbol{\xi}), \tag{2.1}$$

where Ω represents a surface in $\mathbb{R}^3$. Following the notation of [13], we recall the geometrical indicators associated to the mapping (2.1), for which we define the Jacobian of the mapping:

$$\widehat{F} : \widehat{\Omega} \to \mathbb{R}^{3\times 2}, \qquad \boldsymbol{\xi} \to \widehat{F}(\boldsymbol{\xi}), \qquad \widehat{F}_{i,\alpha}(\boldsymbol{\xi}) := \frac{\partial x_i}{\partial \xi_\alpha}(\boldsymbol{\xi}), \qquad i = 1,2,3,\ \alpha = 1,2, \tag{2.2}$$

its first fundamental form:

$$\widehat{G} : \widehat{\Omega} \to \mathbb{R}^{2\times 2}, \qquad \boldsymbol{\xi} \to \widehat{G}(\boldsymbol{\xi}), \qquad \widehat{G}(\boldsymbol{\xi}) := \left(\widehat{F}(\boldsymbol{\xi})\right)^T \widehat{F}(\boldsymbol{\xi}), \tag{2.3}$$

and determinant:

$$\widehat{g} : \widehat{\Omega} \to \mathbb{R}, \qquad \boldsymbol{\xi} \to \widehat{g}(\boldsymbol{\xi}), \qquad \widehat{g}(\boldsymbol{\xi}) := \sqrt{\det\left(\widehat{G}(\boldsymbol{\xi})\right)}. \tag{2.4}$$

We assume the geometrical mapping (2.1) to be invertible a.e. in $\widehat{\Omega}$, i.e. we require $\widehat{g}(\boldsymbol{\xi}) > 0$ *a.e.* in $\widehat{\Omega}$ and allow $\widehat{g}(\boldsymbol{\xi}) = 0$ only in subsets of $\widehat{\Omega}$ with zero measure in the topology of $\mathbb{R}^2$. We can thus

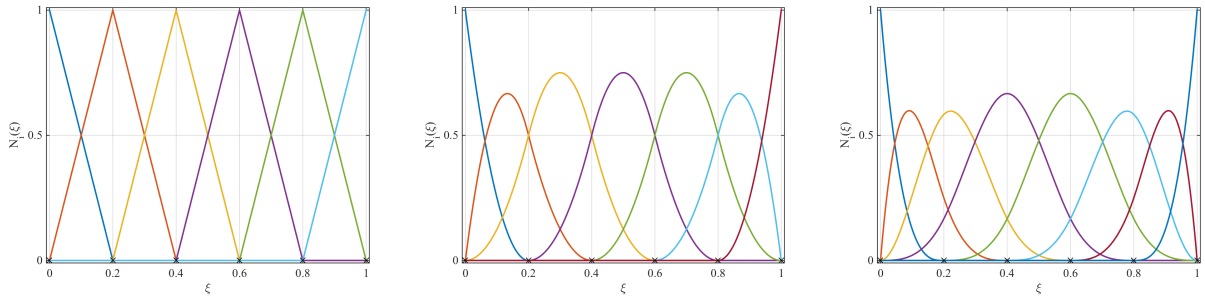

(a) $p = 1$ (b) $p = 2$ (c) $p = 3$

Figure 1: Univariate B-spline basis functions of polynomial degrees $p = 1$, 2, and 3 obtained from the knot vectors $\Xi = \left\{ \{0\}^{p+1}, \frac{1}{5}, \frac{2}{5}, \frac{3}{5}, \frac{4}{5}, \{1\}^{p+1} \right\}$ and globally C^{p-1}-continuous in $\widehat{\Omega} = (0, 1)$.

rewrite the Jacobian, the first fundamental form, and its determinant directly on the manifold Ω as:

$$\begin{aligned} &F : \Omega \to \mathbb{R}^{3\times 2}, \qquad &&\mathbf{x} \to F(\mathbf{x}), \qquad &&F(\mathbf{x}) := \widehat{F}(\boldsymbol{\xi}) \circ \mathbf{x}^{-1}(\boldsymbol{\xi}), \\ &G : \Omega \to \mathbb{R}^{2\times 2}, \qquad &&\mathbf{x} \to G(\mathbf{x}), \qquad &&G(\mathbf{x}) := \widehat{G}(\boldsymbol{\xi}) \circ \mathbf{x}^{-1}(\boldsymbol{\xi}), \\ &g : \Omega \to \mathbb{R}, \qquad &&\mathbf{x} \to g(\mathbf{x}), \qquad &&g(\mathbf{x}) := \widehat{g}(\boldsymbol{\xi}) \circ \mathbf{x}^{-1}(\boldsymbol{\xi}). \end{aligned} \tag{2.5}$$

In this work, we specifically consider surfaces represented by NURBS [31]. Therefore, the geometrical mapping (2.1) reads:

$$\mathbf{x}(\boldsymbol{\xi}) = \sum_{i=1}^{n_{bf}} \widehat{R}_i(\boldsymbol{\xi}) \mathbf{P}_i, \qquad \widehat{R}_i(\boldsymbol{\xi}) := \frac{w_i}{\sum_{j=1}^{n_{bf}} w_j \widehat{N}_j(\boldsymbol{\xi})} \widehat{N}_i(\boldsymbol{\xi}) \qquad \text{for } i = 1, \dots, n_{bf}, \tag{2.6}$$

where $\mathbf{P}_i \in \mathbb{R}^3, i = 1, \dots, n_{bf}$, are the *control points* in the physical space and $\widehat{R}_i(\boldsymbol{\xi})$ are the NURBS basis functions, obtained by projective transformations of the B-spline basis functions $\widehat{N}_i(\boldsymbol{\xi})$ for $i = 1, \dots, n_{bf}$, with weights $w_i \in \mathbb{R}$ and n_{bf} the number of basis functions. The inclusion of weights in the construction of the basis functions is necessary to exactly represent geometries as conic sections, for which B-spline basis functions cannot be used. Without entering into details, the multivariate B-spline basis functions $\widehat{N}_i(\boldsymbol{\xi})$ are obtained from the tensor product of univariate B-spline basis functions, namely $\widehat{N}_{i,\alpha}$ for $i = 1, \dots, n_{bf,\alpha}$, where $\alpha = 1, 2$ refers to the parametric direction; therefore, we have $n_{bf} = n_{bf,1} n_{bf,2}$. The univariate basis functions $\widehat{N}_{i,\alpha}(\xi_\alpha)$ are built using the *Cox-de Boor* recursion formula [31] applied to the *knot vectors* $\Xi_\alpha := \{\xi_{\alpha,j}\}_{j=1}^{n_{bf,\alpha}+p_\alpha+1}$, where $\xi_{\alpha,j} \in \mathbb{R}$ are the *knots* and p_α is the polynomial degree along the parametric direction α. In Figure 1 examples of B-spline basis functions with different polynomial degrees are shown. We recall that the knot vectors define all the properties of the B-spline basis functions in the parametric domain, describing how it is divided into *knot spans*. Therefore, by exploiting the tensor product of the knot vectors, it is possible to define a partition of the parametric domain into subregions, which are called *mesh elements* (in analogy with the FEM). We remark that the main advantage of B-splines and NURBS is the ability to control the continuity of the basis functions; indeed, by changing the multiplicity of a knot inside the knot vector Ξ_α, it is possible to tweak the continuity of the basis functions across that knot. Specifically, if a knot is repeated k times, the basis functions

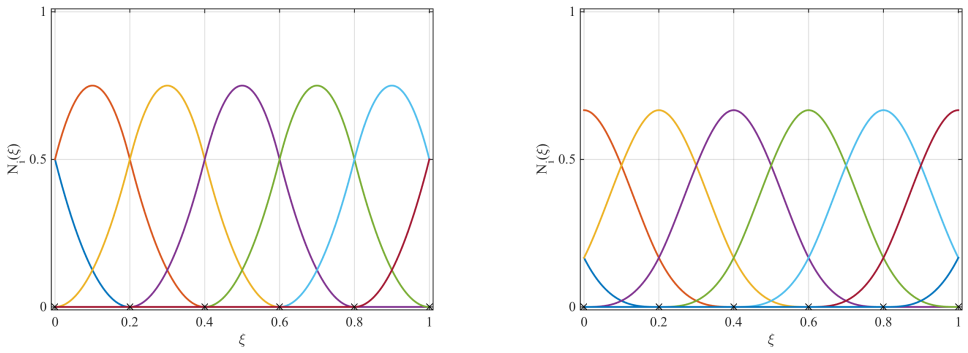

(a) $p = 2$, globally C^1-continuous (b) $p = 3$, globally C^2-continuous

Figure 2: Periodic univariate B-spline basis functions.

are consequently C^{p-k}-continuous across that knot; if a knot is repeated p times, the basis functions are only C^0-continuous across that knot. For a more complete description of B-splines and NURBS we refer the reader to [11, 31].

2.2 NURBS function spaces

We define the NURBS function space $\widehat{\mathcal{N}}_h$ over the parametric domain $\widehat{\Omega}$ as:

$$\widehat{\mathcal{N}}_h := \text{span}\left\{\widehat{R}_i, \quad i = 1, \dots, n_{bf}\right\} \tag{2.7}$$

and its counterpart in the physical domain Ω as:

$$\mathcal{N}_h := \text{span}\left\{\widehat{R}_i(\boldsymbol{\xi}) \circ \mathbf{x}^{-1}(\boldsymbol{\xi}), \quad i = 1, \dots, n_{bf}\right\}. \tag{2.8}$$

According to the isogeometric concept, these spaces will be used to build the trial function spaces for the approximation of PDEs. The subscript h refers to the characteristic size of the mesh elements, and is usually defined as the maximum diameter of the mesh elements in the physical space [13]. We remark that the computational domain Ω is usually represented at its coarsest level of discretization, from which the spaces $\widehat{\mathcal{N}}_h$ and $\mathcal{N}_h$ are built; the coarsest approximation is therefore already suitable to reproduce the surface geometry. For NURBS, there are three different kinds of refinement procedures which permit the enrichment of the NURBS function spaces [11]. Among these, the *knot insertion* refers to the procedure of splitting the knot spans by introducing new knots, effectively increasing the number of mesh elements and basis functions; when the continuity between elements is preserved, inserting knots with the correct multiplicity can be compared to the *h-refinement* procedure of the FEM. The process of increasing the polynomial degree of the basis functions while preserving the existing continuity across the edges of the elements, is called *order elevation* and it is closely related to the FEM *p-refinement*. Finally, B-splines and NURBS benefit from another form of refinement, which does not have counterparts in FEM, the *k-refinement*, for which the degree of the basis functions is firstly elevated and then new unique knots are inserted, maintaining the highest possible continuity across the elements. All these refinement procedures must preserve the original representation of the underlying geometry while enriching the dimension and approximation properties of the function space. For a detailed description, we refer the reader to [11, 25, 31].

When considering closed or partially closed surfaces, as a sphere, cylinder, or torus, the parametrization is such that the NURBS basis functions are only C^0-continuous in $\widehat{\Omega}$ and Ω. Nevertheless, one may be interested in considering NURBS spaces $\mathcal{N}_h$ for which the basis functions feature higher continuity degree over the surface. As we will discuss in Section 4, this is beneficial for the numerical approximation of high order PDEs. In order to build such basis functions, one can apply local linear transformations to the NURBS basis functions originally used to represent the surface, leading to a subparametric approach. Such smooth basis functions can be defined by suitably using the k-refinement procedure and enforcing periodic conditions on the original basis functions. Following the procedure outlined in [27], we define a periodic NURBS function space by applying a transformation linear operator $\mathbf{T}^{per} \in \mathbb{R}^{n_{bf} \times n_{bf}}$ to the basis functions $\widehat{\mathbf{R}} := \left\{ \widehat{R}_i \right\}_{i=1}^{n_{bf}}$ which define the NURBS space $\widehat{\mathcal{N}}_h$, as:

$$\widehat{\mathbf{R}}^{per} := \mathbf{T}^{per} \widehat{\mathbf{R}}(\boldsymbol{\xi}), \tag{2.9}$$

thus obtaining a set of periodic basis functions $\widehat{\mathbf{R}}^{per}$ by enforcing suitable master-slave constraints among the DOFs. The periodic NURBS function spaces are then constructed as:

$$\widehat{\mathcal{N}}_h^{per} := \text{span} \left\{ \widehat{R}_i^{per}, \quad i = 1, \dots, n_{bf} \right\} \tag{2.10}$$

and

$$\mathcal{N}_h^{per} := \text{span} \left\{ \widehat{R}_i^{per}(\boldsymbol{\xi}) \circ \mathbf{x}^{-1}(\boldsymbol{\xi}), \quad i = 1, \dots, n_{bf} \right\}. \tag{2.11}$$

Such procedure allows the construction of periodic basis functions preserving high order continuity across the boundaries of the NURBS patch. A similar approach can be used also inside the parametric domain $\widehat{\Omega}$, in order to restore high order continuity not originally set via the knot vector. This is useful in the case of several geometries of interest, such as the sphere or the torus, which, by construction, are often built by basis functions which are only globally C^0-continuous. An example of univariate periodic B-spline basis functions is shown in Figure 2. For a more detailed description we refer the reader to [11].

3 High Order PDEs on Surfaces

In this section we present the surface differential operators and elliptic high order Laplace-Beltrami operators, which define the high order surface PDEs.

3.1 Surface differential operators

We start by defining a set of differential operators on the surface Ω. Since we consider geometrical mappings (2.1) which are invertible a.e. in $\widehat{\Omega}$, we can take a general, sufficiently regular function on the manifold Ω, e.g. $\phi \in C^0(\Omega)$, and rewrite it in the parametric domain $\widehat{\Omega}$ as:

$$\phi(\mathbf{x}) = \widehat{\phi}(\boldsymbol{\xi}) \circ \mathbf{x}^{-1}(\boldsymbol{\xi}), \tag{3.1}$$

where $\widehat{\phi}(\boldsymbol{\xi}) := \phi\left(\mathbf{x}(\boldsymbol{\xi})\right)$. Surface differential operators can therefore be defined as projection onto the surface of the corresponding differential operators defined in the physical space [4, 6, 14]. Let us now consider a generic function $\phi \in C^1(\Omega)$ and its smooth prolongation $\tilde{\phi}(\mathbf{x})$ from Ω into a "tubular" region in $\mathbb{R}^3$ containing Ω. We can then define the projection tensor $\mathrm{P}(\mathbf{x}) \in \mathbb{R}^{3\times 3}$:

$$\mathrm{P}(\mathbf{x}) := I - \mathbf{n}_\Omega(\mathbf{x}) \otimes \mathbf{n}_\Omega(\mathbf{x}) \qquad \text{for } \mathbf{x} \in \Omega \tag{3.2}$$

where I is the identity tensor in $\mathbb{R}^{3\times 3}$ and $\mathbf{n}_\Omega(\mathbf{x})$ is the unit vector normal to the surface Ω, namely the mapping of:

$$\hat{\mathbf{n}}_\Omega(\boldsymbol{\xi}) := \frac{\hat{\mathbf{t}}_{\Omega,1}(\boldsymbol{\xi}) \times \hat{\mathbf{t}}_{\Omega,2}(\boldsymbol{\xi})}{|\hat{\mathbf{t}}_{\Omega,1}(\boldsymbol{\xi}) \times \hat{\mathbf{t}}_{\Omega,2}(\boldsymbol{\xi})|}, \tag{3.3}$$

where $\hat{\mathbf{t}}_{\Omega,\alpha}(\boldsymbol{\xi}) := \dfrac{\partial \mathbf{x}}{\partial \xi_\alpha}(\boldsymbol{\xi})$, for $\alpha = 1, 2$, are the unit vectors tangent to the surface. Then, we obtain the surface gradient as:

$$\nabla_\Omega \phi(\mathbf{x}) := \left[\mathrm{P}\, \nabla \tilde{\phi}(\mathbf{x})\right] = \nabla \tilde{\phi}(\mathbf{x}) - \left(\nabla \tilde{\phi}(\mathbf{x}) \cdot \mathbf{n}_\Omega(\mathbf{x})\right) \mathbf{n}_\Omega(\mathbf{x}) \qquad \text{for } \mathbf{x} \in \Omega, \tag{3.4}$$

which is rewritten using the geometrical mapping (2.1) and Eqs. (2.2) and (2.3) as:

$$\nabla_\Omega \phi(\mathbf{x}) = \left[\widehat{F}(\boldsymbol{\xi}) \widehat{G}^{-1}(\boldsymbol{\xi}) \widehat{\nabla} \widehat{\phi}(\boldsymbol{\xi})\right] \circ \mathbf{x}^{-1}(\boldsymbol{\xi}) \qquad \text{for } \mathbf{x} \in \Omega, \tag{3.5}$$

where $\widehat{\nabla}\widehat{\phi}(\boldsymbol{\xi}) : \widehat{\Omega} \to \mathbb{R}^2$ is the gradient operator in the parameter domain. Similarly, by considering a vector field $\mathbf{v} \in \left[C^1(\Omega)\right]^3$ we can define its surface divergence as:

$$\nabla_\Omega \cdot \mathbf{v}(\mathbf{x}) = \mathrm{trace}\left(\nabla_\Omega \mathbf{v}(\mathbf{x})\right) \qquad \text{for } \mathbf{x} \in \Omega, \tag{3.6}$$

which is rewritten using Eqs. (2.2), (2.3), and (2.4) as:

$$\nabla_\Omega \cdot \mathbf{v}(\mathbf{x}) = \left[\frac{1}{\widehat{g}(\boldsymbol{\xi})} \widehat{\nabla} \cdot \left(\widehat{g}(\boldsymbol{\xi}) \widehat{G}^{-1}(\boldsymbol{\xi}) \widehat{F}^T(\boldsymbol{\xi}) \hat{\mathbf{v}}(\boldsymbol{\xi})\right)\right] \circ \mathbf{x}^{-1}(\boldsymbol{\xi}) \qquad \text{for } \mathbf{x} \in \Omega, \tag{3.7}$$

where $\hat{\mathbf{v}}(\boldsymbol{\xi}) := \mathbf{v}\left(\mathbf{x}(\boldsymbol{\xi})\right)$. For a function $\phi \in C^2(\Omega)$ we can compose the surface divergence operator (3.6) with the surface gradient operator (3.4) to define the Laplace-Beltrami operator on the manifold Ω as:

$$\Delta_\Omega \phi(\mathbf{x}) := \nabla_\Omega \cdot \left(\nabla_\Omega \phi(\mathbf{x})\right) = \mathrm{trace}\left[\mathrm{P}(\mathbf{x}) \nabla^2 \tilde{\phi}(\mathbf{x})\, \mathrm{P}(\mathbf{x})\right] \qquad \text{for } \mathbf{x} \in \Omega, \tag{3.8}$$

where ∇^2 is the Hessian operator, such that $\left(\nabla^2 \tilde{\phi}(\mathbf{x})\right)_{i,j} := \dfrac{\partial^2 \tilde{\phi}}{\partial x_i \partial x_j}(\mathbf{x})$ for $i, j = 1, 2, 3$. Then, Eq. (3.8) is rewritten in terms of the geometrical mapping (2.1) as:

$$\Delta_\Omega \phi(\mathbf{x}) = \left[\frac{1}{\widehat{g}(\boldsymbol{\xi})} \widehat{\nabla} \cdot \left(\widehat{g}(\boldsymbol{\xi})\, \widehat{G}^{-1}(\boldsymbol{\xi})\, \widehat{\nabla} \widehat{\phi}(\boldsymbol{\xi})\right)\right] \circ \mathbf{x}^{-1}(\boldsymbol{\xi}) \qquad \text{for } \mathbf{x} \in \Omega. \tag{3.9}$$

Finally, in order to consider sixth order PDEs on surfaces, we need the gradient of Laplace-Beltrami operator on the surface. For a function $\phi \in C^3(\Omega)$, we can write this operator as:

$$\nabla_\Omega \Delta_\Omega \phi(\mathbf{x}) := \nabla_\Omega \left(\Delta_\Omega \phi(\mathbf{x})\right) = \mathrm{P}(\mathbf{x}) \nabla \left(\mathrm{trace}\left[\mathrm{P}(\mathbf{x}) \nabla^2 \tilde{\phi}(\mathbf{x})\, \mathrm{P}(\mathbf{x})\right]\right) \qquad \text{for } \mathbf{x} \in \Omega, \tag{3.10}$$

which is rewritten using the geometrical mapping (2.1) and Eqs. (2.2), (2.3), and (2.4) as:

$$\nabla_\Omega \Delta_\Omega \phi(\mathbf{x}) = \left[\widehat{F}(\boldsymbol{\xi}) \widehat{G}^{-1}(\boldsymbol{\xi}) \widehat{\nabla} \left(\frac{1}{\widehat{g}(\boldsymbol{\xi})} \widehat{\nabla} \cdot \left[\widehat{g}(\boldsymbol{\xi}) \widehat{G}^{-1}(\boldsymbol{\xi}) \widehat{\nabla} \widehat{\phi}(\boldsymbol{\xi})\right]\right)\right] \circ \mathbf{x}^{-1}(\boldsymbol{\xi}) \qquad \text{for } \mathbf{x} \in \Omega. \tag{3.11}$$

3.2 High order PDEs

Let us consider a surface $\Omega \subset \mathbb{R}^3$ described by NURBS and a scalar elliptic PDE of order $2m$, with $m = 1$, 2, or 3. In general, its weak formulation reads:

$$\text{find } u \in V_g \quad : \quad a(v,u) = F(v) \qquad \forall v \in V_0, \tag{3.12}$$

where $a : V_0 \times V_g \to \mathbb{R}$ is a continuous and strongly coercive bilinear form associated to one of the surface differential operators (3.4), (3.8), or (3.10), $F : V_0 \to \mathbb{R}$ is a continuous linear functional, V_g and V_0 are suitable Hilbert spaces, subsets of $H^m(\Omega)$ (V_g and $V_0 \subseteq H^m(\Omega)$), with V_0 yielding the homogeneous counterpart of the essential boundary conditions, while V_g the non-homogeneous counterpart. Thanks to the Lax-Milgram Lemma [33], the solution of Eq. (3.12) exists and is unique. If the domain Ω is a closed surface, Ω does not possess boundary and we can consider $V = V_g = V_0$; in this case, the weak formulation of a generic scalar elliptic PDE of order $2m$ reads:

$$\text{find } u \in V \quad : \quad a(v,u) = F(v) \qquad \forall v \in V, \tag{3.13}$$

where we assume that the form $a : V \times V \to \mathbb{R}$ carries a zeroth order linear operator corresponding to a dissipation term, which makes $a(\cdot,\cdot)$ strongly coercive in $V \equiv H^m(\Omega)$.

By recalling the invertibility of the geometric mapping (2.1), we recast problems (3.12) and (3.13) into the parametric domain $\widehat{\Omega}$, thus obtaining:

$$\text{find } \widehat{u} \in \widehat{V}_g \quad : \quad \widehat{a}(\widehat{v},\widehat{u}) = \widehat{F}(\widehat{v}) \qquad \forall \widehat{v} \in \widehat{V}_0 \tag{3.14}$$

and

$$\text{find } \widehat{u} \in \widehat{V} \quad : \quad \widehat{a}(\widehat{v},\widehat{u}) = \widehat{F}(\widehat{v}) \qquad \forall \widehat{v} \in \widehat{V}, \tag{3.15}$$

respectively, where $\widehat{V}_g$, $\widehat{V}_0$, and $\widehat{V}$ correspond to the spaces V_g, V_0, and V defined over the parametric domain $\widehat{\Omega}$. This operation of recasting the problem in $\widehat{\Omega}$ is usually called *pull-back* operation and it is performed by exploiting the differential operators (3.5), (3.7), (3.9), and (3.11) introduced in the previous section to build the form $\widehat{a}(\cdot,\cdot)$ and the functional $\widehat{F}(\cdot)$.

3.2.1 Laplace-Beltrami biharmonic problem

Let us consider a sufficiently regular open surface domain $\Omega \subset \mathbb{R}^3$ described by NURBS. The *biharmonic operator* $\Delta^2_\Omega \cdot$ is the fourth order Laplace-Beltrami differential operator on the surface Ω defined as $\Delta^2_\Omega \cdot := \Delta_\Omega \, \Delta_\Omega \cdot$ (here $m = 2$). We consider the following biharmonic problem with homogeneous essential boundary conditions:

$$\text{find } u : \Omega \to \mathbb{R} \quad : \quad \begin{cases} \mu \Delta^2_\Omega u + \gamma u = f & \text{in } \Omega, \\ u = 0 & \text{on } \partial\Omega, \\ \nabla_\Omega u \cdot \mathbf{n} = 0 & \text{on } \partial\Omega, \end{cases} \tag{3.16}$$

where μ and $\gamma \in \mathbb{R}$ are positive constants, $\mathbf{n}$ is the outward directed unit normal vector at the boundary $\partial\Omega$, and f is a sufficiently regular function. If the domain Ω is a closed surface, problem (3.16) reduces to:

$$\text{find } u : \Omega \to \mathbb{R} \quad : \quad \mu \Delta^2_\Omega u + \gamma u = f \qquad \text{in } \Omega. \tag{3.17}$$

Problems (3.16) and (3.17) in weak formulation read as in Eqs. (3.12) and (3.13), now with:

$$a(v,u) := \int_\Omega \mu \, \Delta_\Omega u \, \Delta_\Omega v \, d\Omega + \int_\Omega \gamma \, u \, v \, d\Omega, \tag{3.18}$$

and

$$F(v) := \int_\Omega f\, v\, d\Omega, \tag{3.19}$$

with $V_g = V_0 = H_0^2(\Omega)$ and $V = H^2(\Omega)$, respectively[1]. We recall that problem (3.16) is well posed with $\gamma = 0$, while problem (3.17) necessitates $\gamma > 0$. The problems are then recast into the parametric domain $\widehat{\Omega}$ as in Eqs. (3.14) and (3.15), with the bilinear form $\widehat{a}(\cdot,\cdot)$ and linear operator $\widehat{F}(\cdot)$ obtained by pulling-back $a(\cdot,\cdot)$ and $F(\cdot)$ into the parametric domain $\widehat{\Omega}$ as:

$$\widehat{a}(\widehat{v},\widehat{u}) := \int_{\widehat{\Omega}} \mu\, \frac{1}{\widehat{g}} \widehat{\nabla}\cdot\left(\widehat{g}\,\widehat{G}^{-1}\widehat{\nabla}\widehat{u}\right)\, \widehat{\nabla}\cdot\left(\widehat{g}\,\widehat{G}^{-1}\widehat{\nabla}\widehat{v}\right)\, d\widehat{\Omega} + \int_{\widehat{\Omega}} \gamma\, \widehat{u}\,\widehat{v}\,\widehat{g}\, d\widehat{\Omega}, \tag{3.20}$$

and

$$\widehat{F}(\widehat{v}) := \int_{\widehat{\Omega}} \widehat{f}\,\widehat{v}\,\widehat{g}\, d\widehat{\Omega}. \tag{3.21}$$

3.2.2 Laplace-Beltrami triharmonic problem

The *triharmonic operator* $\Delta_\Omega^3 \cdot$ is the sixth order Laplace-Beltrami differential operator on the surface Ω defined as $\Delta_\Omega^3 \cdot := \Delta_\Omega\, \Delta_\Omega\, \Delta_\Omega \cdot$ (here $m = 3$). We consider the following triharmonic problem with homogeneous essential boundary conditions:

$$\text{find } u : \Omega \to \mathbb{R} \;\; : \;\; \begin{cases} -\mu\Delta_\Omega^3 u + \gamma u = f & \text{in } \Omega, \\ u = 0 & \text{on } \partial\Omega, \\ \nabla_\Omega u \cdot \mathbf{n} = 0 & \text{on } \partial\Omega, \\ \Delta_\Omega u = 0 & \text{on } \partial\Omega, \end{cases} \tag{3.22}$$

where μ and $\gamma \in \mathbb{R}$ are positive constants and f is a sufficiently regular function. When considering closed surface domains, the problem becomes:

$$\text{find } u : \Omega \to \mathbb{R} \;\; : \;\; -\mu\Delta_\Omega^3 u + \gamma u = f \qquad \text{in } \Omega. \tag{3.23}$$

Problems (3.22) and (3.23) in weak formulation read as in Eqs. (3.12) and (3.13), now with:

$$a(v,u) = \int_\Omega \mu\, \nabla_\Omega\left(\Delta_\Omega u\right)\cdot\nabla_\Omega\left(\Delta_\Omega v\right) d\Omega + \int_\Omega \gamma\, u\, v\, d\Omega \tag{3.24}$$

and

$$F(v) = \int_\Omega f\, v\, d\Omega \tag{3.25}$$

respectively, with $V_g = V_0 = H_0^3(\Omega)$ and $V = H^3(\Omega)$. We remark that problem (3.22) is well posed for $\gamma = 0$, while problem (3.23) requires $\gamma > 0$. When recast into the parametric domain $\widehat{\Omega}$, the weak formulations of problems (3.22) and (3.23) read as in Eqs. (3.14) and (3.15), with the bilinear form $\widehat{a}(\cdot,\cdot)$ and linear operator $\widehat{F}(\cdot)$ defined as:

$$\widehat{a}(\widehat{v},\widehat{u}) := \int_{\widehat{\Omega}} \mu\, \widehat{\nabla}\left[\frac{1}{\widehat{g}}\,\widehat{\nabla}\cdot\left(\widehat{g}\,\widehat{G}^{-1}\,\widehat{\nabla}\widehat{u}\right)\right]\cdot\left\{\widehat{G}^{-1}\,\widehat{\nabla}\left[\frac{1}{\widehat{g}}\,\widehat{\nabla}\cdot\left(\widehat{g}\,\widehat{G}^{-1}\,\widehat{\nabla}\widehat{v}\right)\right]\right\}\widehat{g}\, d\widehat{\Omega} + \int_{\widehat{\Omega}} \gamma\,\widehat{u}\,\widehat{v}\,\widehat{g}\, d\widehat{\Omega} \tag{3.26}$$

and

$$\widehat{F}(v) := \int_{\widehat{\Omega}} \widehat{f}\,\widehat{v}\,\widehat{g}\, d\widehat{\Omega}. \tag{3.27}$$

[1] We recall that $H_0^m(\Omega) := \{v : \Omega \to \mathbb{R}, v \in H^m(\Omega), \gamma_0 v = \ldots = \gamma_{m-1} v = 0 \text{ on } \partial\Omega\}$, where γ_k denotes the trace operator of order k, for $k = 0, 1, \ldots, m-1$ [1].

3.2.3 High order Laplace-Beltrami eigenvalue problems

We consider the eigenvalue problem defined on a closed surface Ω, as e.g. the sphere:

$$\text{find } u \in V \text{ and } \lambda \in \mathbb{R} \quad : \quad a(v,u) = \lambda\, b(v,u) \quad \forall v \in V, \tag{3.28}$$

where $a(\cdot,\cdot)$ is the bilinear form associated with either the biharmonic problem (3.18) or the triharmonic problem (3.24) for $\gamma = 0$, while $b : V \times V \to \mathbb{R}$ is the bilinear form representing the mass term, defined as:

$$b(v,u) := \int_\Omega u\, v\, d\Omega \tag{3.29}$$

and $V = H^m(\Omega)$ is a suitable function space chosen according to the order $2m$ of the differential operator as seen in Sections 3.2.1 and 3.2.2. Due to the symmetry of the problem, we expect all the eigenvalues to be real valued and non negative, i.e. $\lambda \in \mathbb{R}, \lambda \geq 0$.

Problem (3.28) can be rewritten into the parametric domain $\widehat{\Omega}$ as:

$$\text{find } \widehat{u} \in \widehat{V} \text{ and } \lambda \in \mathbb{R} \quad : \quad \widehat{a}(\widehat{v},\widehat{u}) = \lambda\, \widehat{b}(\widehat{v},\widehat{u}) \quad \forall \widehat{v} \in \widehat{V}, \tag{3.30}$$

where $\widehat{V}$ is the function space associated to V over the parametric domain $\widehat{\Omega}$, $\widehat{a}(\cdot,\cdot)$ is the bilinear form $a(\cdot,\cdot)$ pulled back into the parametric domain, thus either (3.20), for the biharmonic problem, or (3.26), for the triharmonic problem, for $\gamma = 0$; the bilinear form $\widehat{b} : \widehat{V} \times \widehat{V} \to \mathbb{R}$ reads:

$$\widehat{b}(\widehat{v},\widehat{u}) := \int_{\widehat{\Omega}} \widehat{u}\, \widehat{v}\, \widehat{g}\, d\widehat{\Omega}. \tag{3.31}$$

4 Approximation of PDEs: Isogeometric Analysis

Let us consider as prototype the $2m$-th order PDE (3.12) for $m = 2, 3$ defined on a surface $\Omega \subset \mathbb{R}^3$ described by NURBS. We consider its approximation by means of NURBS-based IGA in the framework of the Galerkin method. We thus use the NURBS function space $\mathcal{N}_h$ defined in Eq. (2.8) and look for an approximate solution $u_h \in \mathcal{N}_h$ such that:

$$u_h(\mathbf{x}) = \sum_{i=1}^{n_{bf}} \left(\widehat{R}_i(\boldsymbol{\xi}) \circ \mathbf{x}^{-1}(\boldsymbol{\xi}) \right) U_i, \tag{4.1}$$

where $\mathbf{U} = \left(U_1, \ldots, U_{n_{bf}}\right)^T \in \mathbb{R}^{n_{bf}}$ is the vector of *control variables*, corresponding to the unknowns of the discrete problem. For IGA in the framework of the Galerkin method, u_h is obtained by solving the finite dimensional problem:

$$\text{find } u_h \in V_{g,h} \quad : \quad a(v_h,u_h) = F(v_h) \qquad \forall v_h \in V_{0,h}, \tag{4.2}$$

where $V_{g,h} := V_g \cap \mathcal{N}_h$ and $V_{0,h} := V_0 \cap \mathcal{N}_h$. Then, we rewrite it in the parametric domain $\widehat{\Omega}$, obtaining:

$$\text{find } \widehat{u}_h \in \widehat{V}_{g,h} \quad : \quad \widehat{a}\,(\widehat{v}_h,\widehat{u}_h) = \widehat{F}\,(\widehat{v}_h) \qquad \forall \widehat{v}_h \in \widehat{V}_{0,h}, \tag{4.3}$$

where $\widehat{V}_{g,h} := \widehat{V}_g \cap \widehat{\mathcal{N}}_h$ and $\widehat{V}_{0,h} := \widehat{V}_0 \cap \widehat{\mathcal{N}}_h$. The transformed solution $\widehat{u}_h$ reads:

$$\widehat{u}_h(\boldsymbol{\xi}) = \sum_{i=1}^{n_{bf}} \widehat{R}_i(\boldsymbol{\xi})\, U_i. \tag{4.4}$$

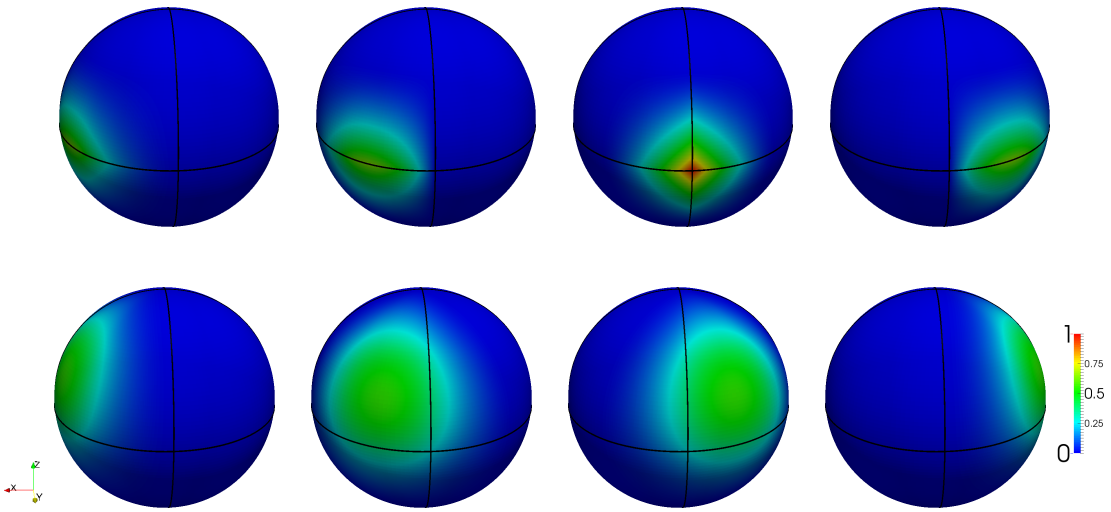

Figure 3: Examples of NURBS basis functions of degree $p = 2$ on the sphere; globally C^0-continuous basis functions (top row) and C^2-continuous a.e. basis functions (bottom row).

The same procedure is followed when considering problems defined on closed surfaces, like (3.13). The high order Laplace-Beltrami eigenvalue problem defined in (3.28) is discretized by means of NURBS-based IGA in a similar way; in the parametric domain $\widehat{\Omega}$, it reads:

$$\text{find } \widehat{u}_h \in \widehat{V}_h \text{ and } \lambda_h \in \mathbb{R} \quad : \quad \widehat{a}(\widehat{v}_h, \widehat{u}_h) = \lambda_h \widehat{b}(\widehat{v}_h, \widehat{u}_h) \qquad \forall \widehat{v}_h \in \widehat{V}_h, \tag{4.5}$$

where $\widehat{a}(\cdot,\cdot)$ is either the bilinear form (3.20) or (3.26), $\widehat{b}(\cdot,\cdot)$ is the bilinear form of Eq. (3.31), and $\widehat{V}_h$ is a suitable NURBS function space whose elements satisfy the differentiability requirements associated to the operators under consideration (that is $H_0^m(\widehat{\Omega})$ or $H^m(\widehat{\Omega})$ for an original differential operator of order $2m$).

We remark that, depending on the order of the PDE, it is necessary to satisfy different differentiability requirements on u_h and v_h. Specifically, for PDEs of order $2m$ the trial and test function spaces should be subspaces of the function space $H^m(\Omega)$, for $m \geq 1$. This requirement is satisfied for example if the basis functions are at least globally C^{m-1}-continuous on the surface Ω. This is a distinguishing feature of NURBS-based IGA: the global continuity of the NURBS basis functions can be defined and set by means of suitable refinement procedures [40]. As mentioned in Section 2.2, by using a subparametric approach, globally C^{m-1}-continuous basis functions on closed or partially closed surfaces can be defined by using suitable local linear transformations. In these cases, the NURBS spaces for the IGA approximation are built as e.g. $\widehat{V}_h^{per} = \widehat{V} \cap \widehat{\mathcal{N}}_h^{per}$ and $V_h^{per} = V \cap \mathcal{N}_h^{per}$ from Eqs. (2.10) and (2.11). In this respect, we use at least globally C^1-continuous basis functions for fourth order problems ($m = 2$) and at least globally C^2-continuous basis functions for sixth order problems ($m = 3$). However, some closed surfaces of practical interest, as e.g. the sphere, can only be built by NURBS basis functions which do not possess the required degree of global continuity, as the presence of localized singularities of the geometrical mapping prevents the basis functions to be globally C^{m-1}-continuous on Ω. For example, the standard single patch construction of the sphere involves the presence of two singularities at the poles, for which the subparametric approach leads to the use of NURBS spaces where the functions are only C^0-continuous at the poles and up to C^{m-1}-continuous elsewhere. In this case, the basis function

are C^{m-1}-continuous a.e. in Ω and globally C^{m-1}-continuous in $\widehat{\Omega}$. Nevertheless, even in presence of these pointwise singularities, numerical evidence shows that the spaces V_h^{per} obtained in this manner are subspaces of $H^m(\Omega)$ even if the basis functions are not pointwise C^{m-1}-continuous across the poles (see Sections 5.1 and 5.2). As example, in Figure 3 eight NURBS basis functions of degree $p = 2$ on the sphere are reported: the top row shows the original non transformed NURBS basis functions which are only C^0-continuous across the equator and four meridians (indicated as black lines); the bottom row shows four periodic basis functions which have been transformed as in Eq. (2.9) and are C^1-continuous a.e. on the sphere, i.e. except at the poles.

We now briefly discuss the accuracy of the IGA approximation of problem (4.2) under h-refinement. In this respect, in [40] error estimates for the approximation of elliptic high order PDEs by means of NURBS-based IGA are available for 2D and 3D domains. In particular, following Theorem 3.3 of [40] for an elliptic PDE of order $2m$ defined in $\Omega \subset \mathbb{R}^d$, for $d = 2, 3$, endowed with homogeneous essential boundary conditions, let us assume that $u \in H^r(\Omega)$, for $r \geq m$, and that the approximate solution u_h is obtained by means of NURBS-based IGA in the framework of the Galerkin method. Then, we have from [40] the following a priori error estimate in lower order norms $H^\sigma(\Omega)$, with $0 \leq \sigma \leq m$:

$$\|u - u_h\|_{H^\sigma(\Omega)} \leq C_{shape} h^\beta \|u\|_{H^r(\Omega)}, \tag{4.6}$$

where p is the polynomial degree, $\beta := \min\{\delta - \sigma, 2(\delta - m)\}$, with $\delta := \min\{r, p + 1\}$, and C_{shape} being a constant independent of h. We remark that, while the result of [40] is proved for problems for which the dimension of the parametric domain $\widehat{\Omega} \subset \mathbb{R}^k$ is equal to the dimension of the physical domain $\Omega \subset \mathbb{R}^d$, i.e. $k = d$, it can be extended to the case of surfaces, similarly to [13] for second order surface PDEs.

5 Numerical Solution of Steady PDEs

We consider the solution of benchmark problems with fourth and sixth order elliptic PDEs defined on open and closed surfaces. Specifically, we propose two test cases: the numerical approximation of the Laplace-Beltrami biharmonic problem (Test 1) and the Laplace-Beltrami triharmonic problem (Test 2) on a quarter of cylinder (open surface) and a unit sphere (closed surface).

5.1 Test 1. Laplace-Beltrami biharmonic problem

We consider the numerical approximation of the Laplace-Beltrami biharmonic problem (3.16) on a open surface Ω representing a quarter of cylinder (Test 1.1) and then of problem (3.17) on a sphere (Test 1.2). Since $V \subseteq H^2(\Omega)$, for the discretization of the problem (and the exact representation of the geometry) we consider NURBS bases of degree $p \geq 2$ and at least globally C^1-continuous in the parametric domain $\widehat{\Omega}$. Regarding the sphere, we enforce global H^2-regularity in the physical space across the closed surface by means of the periodic transformations of the NURBS basis functions described in Sections 2.2 and 4. We remark that, in this way, we obtain at least global C^{p-1}-continuity a.e. on the surface of the sphere, with exception at the poles.

We consider an hand-crafted right-hand-side function f such that the exact solution u is known and is globally C^∞-continuous on Ω. Specifically, for Test 1.1, with the domain $\Omega = (0, \pi/2) \times (0, 1)$ in cylindrical coordinates representing a quarter of cylinder with unitary radius and centered in the origin, we consider the following exact solution in cylindrical coordinates (ϕ, z) (Figure 4a):

$$u(\phi, z) = \sin^2(2\phi) \sin^2(\pi z), \tag{5.1}$$

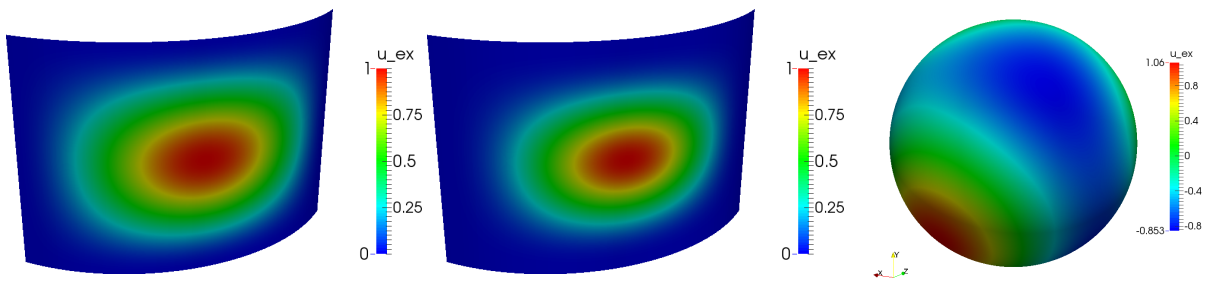

(a) Solution of Test 1.1 (b) Solution of Test 2.1 (c) Solution of Tests 1.2 and 2.2

Figure 4: Exact solutions u of the biharmonic and triharmonic problems (Tests 1 and 2) on a quarter of cylinder and a unit sphere.

where $\phi = \text{atan}(y/z)$, with $\mu = 1$ and $\gamma = 0$. On the sphere of unitary radius centered at the origin (Test 1.2) we use instead (Figure 4c):

$$u(x,y,z) = (x-x_0)(y-y_0)^2 - (y-y_0)(z-z_0)^2 + (x-x_0)^2(z-z_0), \tag{5.2}$$

with $x_0 = 0.05$, $y_0 = 0.1$, and $z_0 = 0.15$.

The biharmonic problem is governed by a fourth order operator ($m = 2$) and, when considering exact solutions $u \in H^r(\Omega)$, with $r \geq m$ (as it is the case with $u \in C^\infty(\Omega)$), the following estimates hold for problem (3.16) as deduced by the inequality (4.6):

$$\begin{aligned} \|u - u_h\|_{H^2(\Omega)} &\leq C_{shape} h^{p-1} \|u\|_{H^r(\Omega)} \\ \|u - u_h\|_{L^2(\Omega)} &\leq \tilde{C}_{shape} h^{\min\{p+1, 2p-2\}} \|u\|_{H^r(\Omega)}. \end{aligned} \tag{5.3}$$

In Figure 5, we report the errors[2] in norms $H^2(\Omega)$ and $L^2(\Omega)$ obtained by the IGA approximation of the biharmonic problem on the quarter of cylinder (Test 1.1) under h-refinement, having used NURBS bases of degree $p = 2$ and $p = 3$, which are globally C^1- and C^2-continuous, respectively. We observe that the convergence rates are in agreement with the error estimates (5.3). Indeed, the convergence rates are 1 and 2 for the errors in norm H^2 using basis of degrees $p = 2$ and 3, respectively; similarly, the rates are 2 and 4 for the errors in the norm L^2 for $p = 2$ and 3, respectively.

The errors obtained for the approximation of the biharmonic problem on the unit sphere (Test 1.2) are reported instead in Figure 6, for which the convergence rates still satisfy Eq. (5.3) (actually, the convergence rate for the error in the lower order norm L^2 is higher than expected from Eq. (5.3) for $p = 2$, being equal to 3). For the sake of comparison, we also consider the approximation of the biharmonic problem (3.17) on the sphere Ω by means of a standard isoparametric FEM. In this case, we consider, in view of the FEM approximation based on C^0-continuous Lagrangian basis functions, the following mixed formulation:

$$\text{find } u, y : \Omega \to \mathbb{R} \quad : \quad \begin{cases} -\Delta_\Omega u - y = 0 & \text{in } \Omega, \\ -\mu \Delta_\Omega y + \gamma u = f & \text{in } \Omega, \end{cases} \tag{5.4}$$

[2]We remark that, instead of computing the norm H^2 by using the full seminorm H^2, we evaluate the norm L^2 of the surface Laplace-Beltrami operator. Indeed, for closed surfaces or open surfaces for which the essential boundary conditions are enforced, these are equivalent, i.e. $\|\Delta_\Omega \varphi\|_{L^2(\Omega)} \simeq |\varphi|_{H^2(\Omega)}$, for $\varphi \in H^2(\Omega)$ on a closed surface or $\varphi \in H^2_0(\Omega)$.

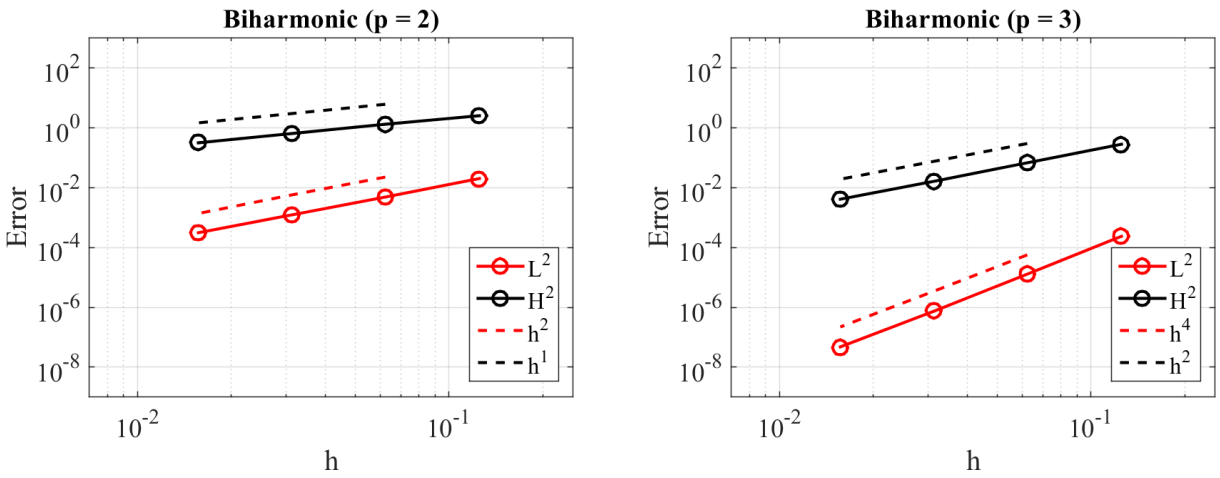

Figure 5: Test 1.1. Biharmonic problem on the quarter of cylinder. Errors in norms $H^2(\Omega)$ and $L^2(\Omega)$ vs. mesh size h for NURBS bases of degrees $p = 2$ and 3, globally C^1- and C^2-continuous, respectively (logarithmic scales are used on both the axes).

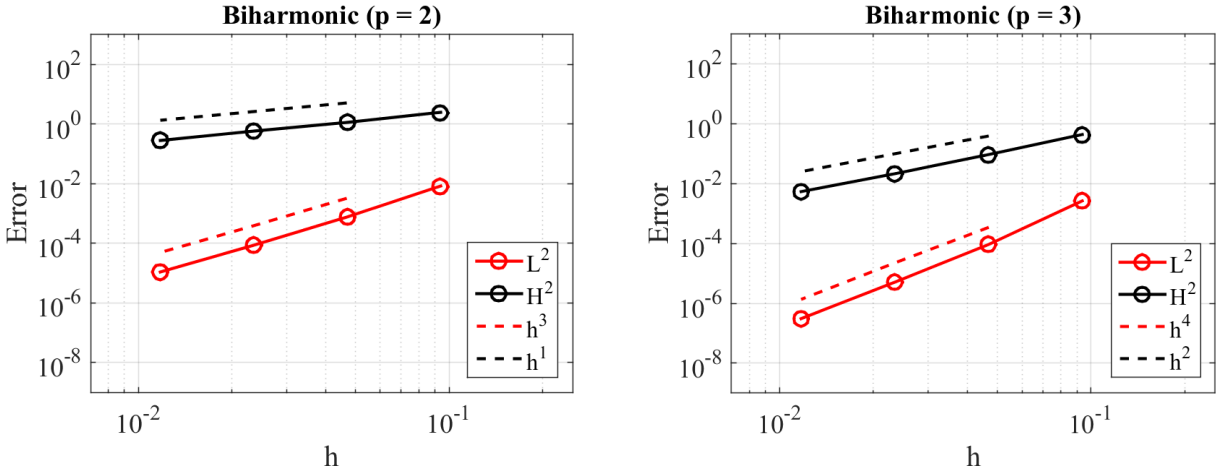

Figure 6: Test 1.2. Biharmonic problem on the sphere. Errors in norms $H^2(\Omega)$ and $L^2(\Omega)$ vs. mesh size h for NURBS bases of degrees $p = 2$ and 3, C^1- and C^2-continuous a.e. on Ω, respectively (logarithmic scales are used on both the axes).

where $y : \Omega \to \mathbb{R}$ is an auxiliary unknown. Problem (5.4), for which u and $y \in H^1(\Omega)$, is discretized using isoparametric FEM of degrees $p = 2$ and 3 on successively finer meshes of the unit sphere. We remark that, due to the difficulty of having high order continuity across the elements, standard FEM discretizations need a system of equations with approximately twice the amount of DOFs compared to IGA, and thus are potentially less efficient. A comparison between the approximation errors obtained with IGA and FEM discretizations is shown in Figure 7, for which both the errors vs. the mesh size and the number of DOFs involved in the IGA and FEM approximations are reported. As we notice from Figure 7, the IGA approximation requires a smaller number of DOFs than its FEM counterpart of the same degree to achieve the same level of error. Thus, the same accuracy can be obtained with less DOFs for which IGA is potentially more efficient than the isoparametric FEM for the approximation of this high order problem.

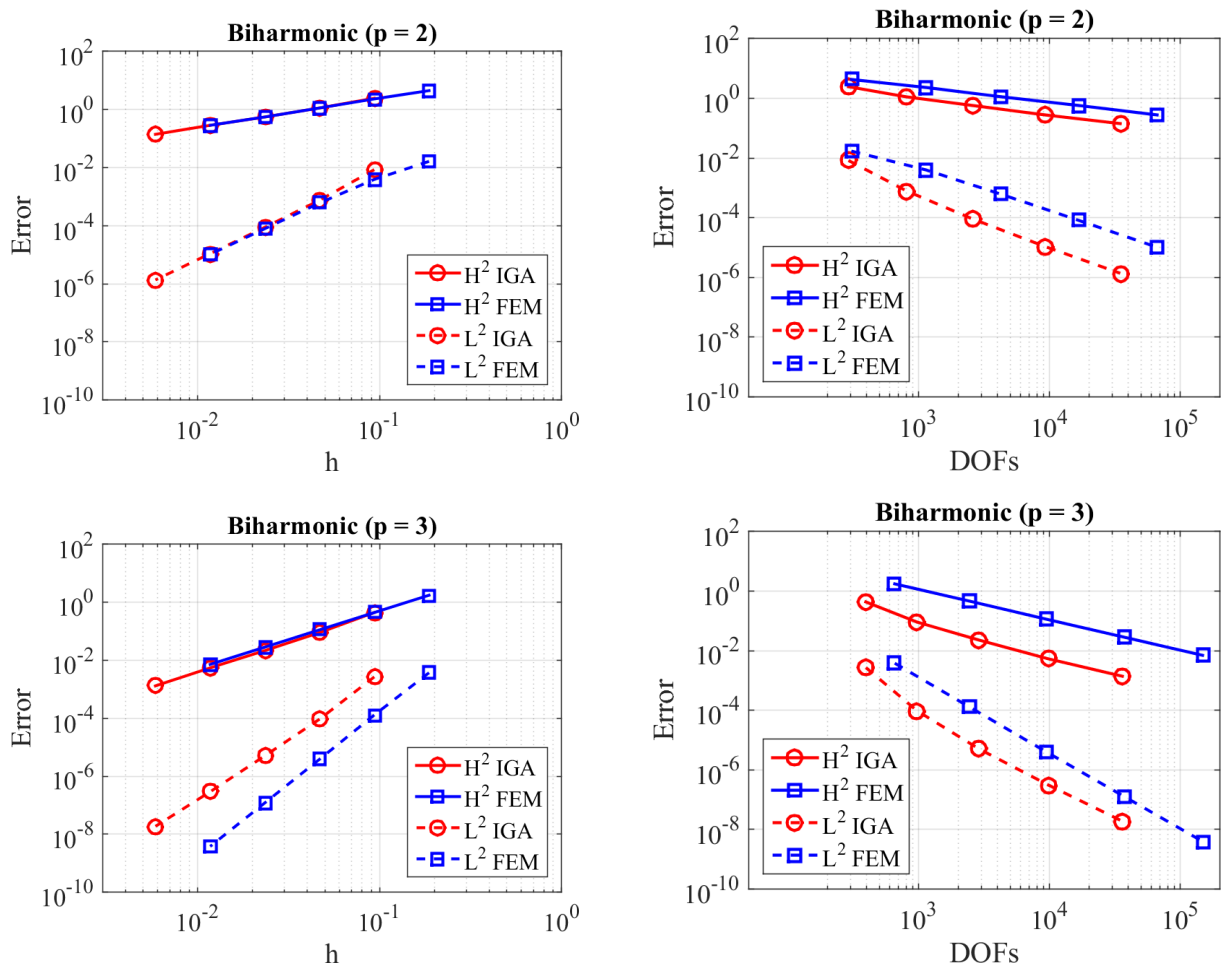

Figure 7: Test 1.2. Biharmonic problem on the sphere. Errors in norms $H^2(\Omega)$ and $L^2(\Omega)$ vs. mesh size h (left) and number of DOFs (right), obtained with IGA and FEM for degrees $p = 2$ (top) and 3 (bottom); the IGA approximation uses NURBS basis functions C^1- and C^2-continuous a.e. on Ω, respectively (logarithmic scales are used on both the axes).

5.2 Test 2. Laplace-Beltrami triharmonic problem

We consider the numerical approximation of problems (3.22) and (3.23) on the quarter of cylinder (Test 2.1) and the unit sphere (Test 2.2), respectively. Following the same procedure outlined in Section 3.2.1, we employ for the discretization of the problem and the representation of the geometry NURBS bases of degree $p \geq 3$ and at least globally C^2-continuous in the parametric domain $\widehat{\Omega}$. For Test 2.1, defined on the quarter of cylinder, we consider the following exact solution in cylindrical coordinates (ϕ, z) (Figure 4b):

$$u(\phi, z) = \sin^3(2\phi)\, \sin^3(\pi z), \tag{5.5}$$

where $\phi = \text{atan}(y/z)$, with $\mu = 1$, and $\gamma = 0$ and f suitably chosen. For problem (3.23) defined on the sphere (Test 2.2), we consider a right-hand-side function f such that the exact solution u is the one reported in Eq. (5.2) and shown in Figure 4c using the same parameters.

By applying Theorem 3.3 of [40] to problem (3.22), an elliptic PDE of order 6 endowed with homogeneous essential boundary conditions, for which $u \in H^r(\Omega)$, with $r \geq 3$, the following

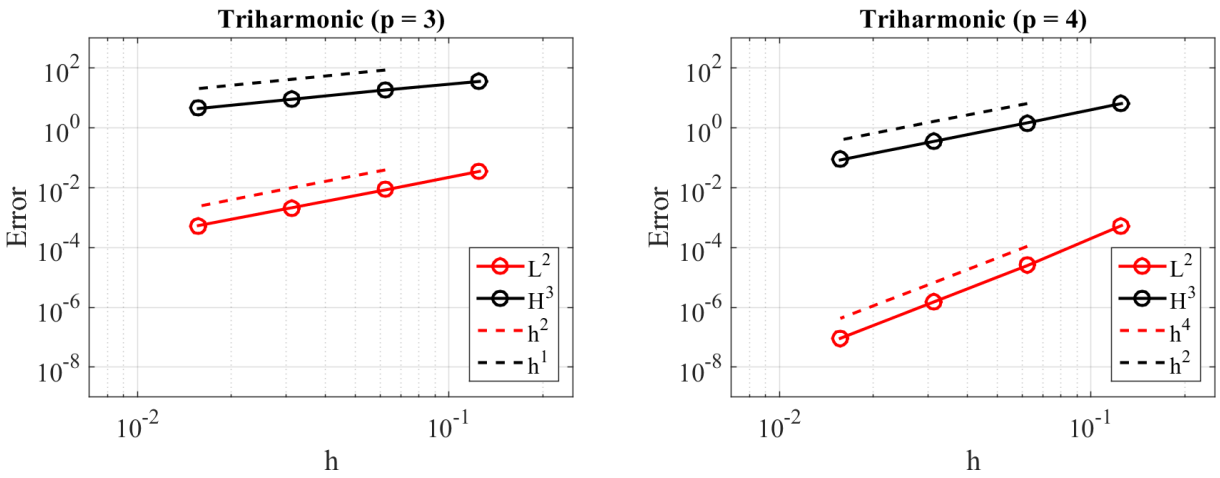

Figure 8: Test 2.1. Triharmonic problem on the quarter of cylinder. Errors in norms $H^3(\Omega)$ and $L^2(\Omega)$ vs. mesh size h for NURBS bases of degree $p = 3$ and 4 and globally C^2-continuous in both cases (logarithmic scales are used on both the axes).

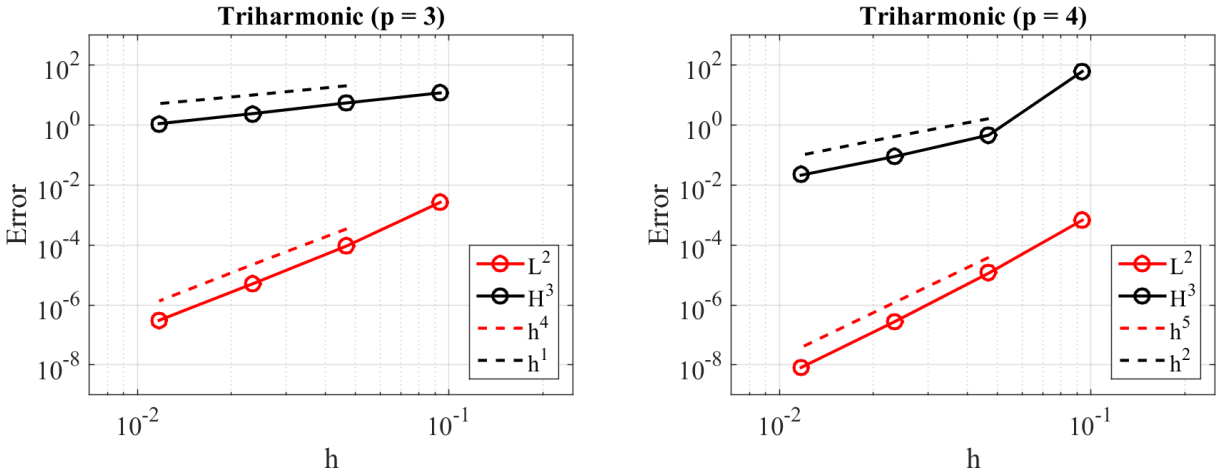

Figure 9: Test 2.2. Triharmonic problem on the sphere. Errors in norms $H^3(\Omega)$ and $L^2(\Omega)$ vs. mesh size h for NURBS bases of degrees $p = 3$ and 4 and C^2-continuous a.e. on Ω in both cases (logarithmic scales are used on both the axes).

estimates hold from Eq. (4.6):

$$\begin{aligned} \|u - u_h\|_{H^3(\Omega)} &\leq C_{shape} h^{p-2} \|u\|_{H^r(\Omega)} \\ \|u - u_h\|_{L^2(\Omega)} &\leq C_{shape} h^{\min\{p+1, 2p-4\}} \|u\|_{H^r(\Omega)}. \end{aligned} \tag{5.6}$$

Figure 8 shows the errors[3] in norms $H^3(\Omega)$ and $L^2(\Omega)$ obtained by the IGA approximation of the triharmonic problem on the quarter of cylinder (Test 2.1) under h-refinement, with C^2-continuous

[3]Similarly to the case of the biharmonic problem, we do not compute the norm H^3 by using the seminorm H^3, but rather we use the norm L^2 of the third order Laplace-Beltrami operator. Indeed, for closed surfaces and problems with essential boundary conditions, the former seminorm and norm are equivalent, i.e. $|\varphi|_{H^3(\Omega)} \simeq \|\nabla_\Omega \Delta_\Omega \varphi\|_{L^2(\Omega)}$, for $\varphi \in H^3(\Omega)$ with Ω closed or $\varphi \in H^3_0(\Omega)$.

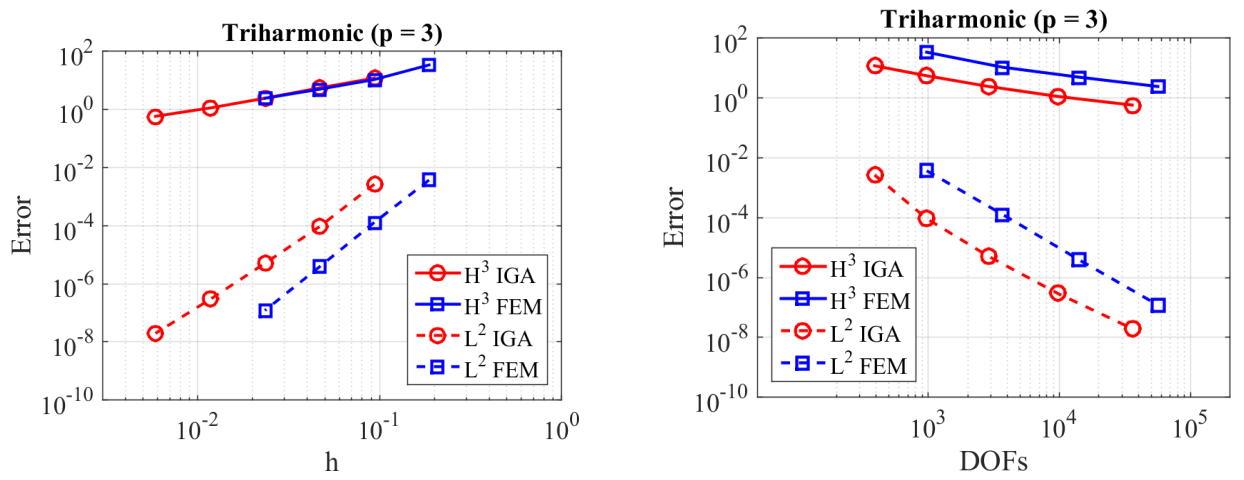

Figure 10: Test 2.2. Triharmonic problem on the sphere. Errors in norm $H^3(\Omega)$ and $L^2(\Omega)$ vs. mesh size h (left) and number of DOFs (right), obtained with IGA and FEM for degree $p = 3$; for the IGA approximation NURBS basis functions C^2-continuous a.e. on Ω are used (logarithmic scales are used on both the axes).

NURBS basis functions of degrees $p = 3$ and 4. We observe that the convergence rates obtained are in agreement with the error estimate (5.6); indeed, the rates are 1 and 2 for the errors in norm H^3 using basis of degrees $p = 3$ and 4, respectively, and 2 and 4 for the errors in norm L^2 for $p = 3$ and 4, respectively.

Figure 9 shows the errors obtained by the numerical approximation of the triharmonic problem on the sphere (Test 2.2). Similarly to the biharmonic problem, the convergence rates of the error in norm L^2 are higher than expected; indeed, these are 4 and 5 using basis of degrees $p = 3$ and 4, respectively. In addition, we consider the approximation of the triharmonic problem (3.23) defined on the sphere Ω by means of a standard isoparametric FEM approximation. In this respect, we consider the problem in mixed formulation:

$$\text{find } u, y, z : \Omega \to \mathbb{R} \quad : \quad \begin{cases} -\Delta_\Omega u + z = 0 & \text{in } \Omega, \\ -\Delta_\Omega z + y = 0 & \text{in } \Omega, \\ -\mu \Delta_\Omega y + \gamma u = f & \text{in } \Omega, \end{cases} \tag{5.7}$$

where y and $z : \Omega \to \mathbb{R}$ are auxiliary unknowns. Problem (5.7) is discretized using isoparametric FEM of degree $p = 3$ on successively finer meshes on the unit sphere. In this case, the FEM discretizations of problem (5.7) yield system of equations with approximately three times the amount of DOFs of IGA. The errors obtained with IGA and FEM are reported in Figure 10 vs. the mesh size and the number of DOFs. As we can observe, IGA yields the same level of error with a much smaller number of DOFs, for which the same accuracy can be obtained more efficiently.

5.3 Test 3. High order Laplace-Beltrami eigenvalue problems

We consider the numerical approximation of the eigenvalue problem (3.30) associated to the Laplace-Beltrami operators of the fourth ($m = 2$) and sixth ($m = 3$) orders on the unit sphere. The exact eigenvalues, solution of the eigenvalue problem governed by an operator of order $2m$,

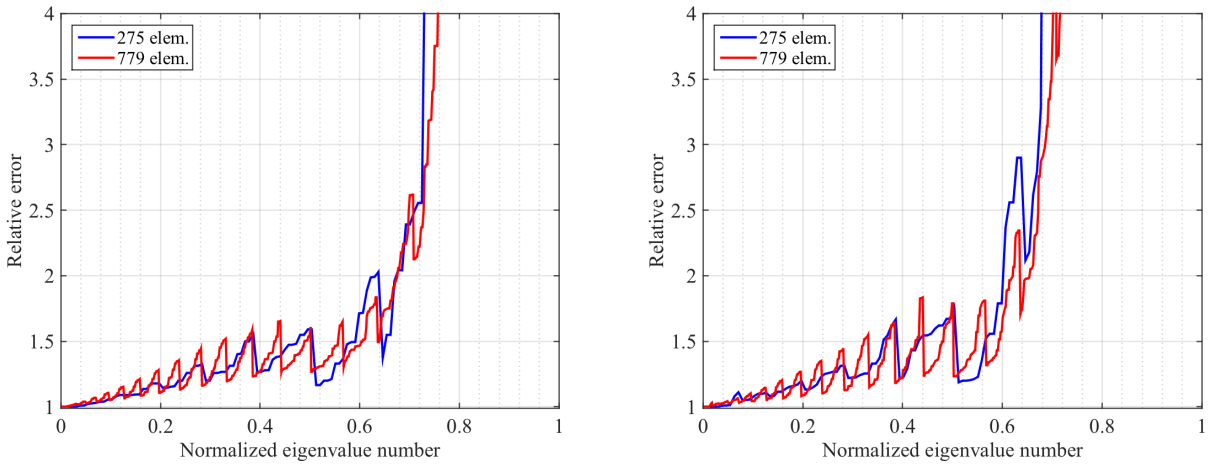

(a) Bilaplacian, $p = 2$, C^1-continuous a.e. (b) Trilaplacian, $p = 3$, C^2-continuous a.e.

Figure 11: Test 3. Laplace-Beltrami eigenvalue problems on the sphere. Normalized spectra computed by solving the bilaplacian and trilaplacian eigenvalue problems, with NURBS bases of degree $p = 2$ and C^1-continuous a.e. in Ω (left) and degree $p = 3$ and C^2-continuous a.e. in Ω (right), respectively.

with $m \geq 1$, are (see e.g. [36]):

$$\lambda_n = (n(n+1))^m \qquad \text{for } n = 0, 1, \ldots, \infty, \tag{5.8}$$

where each eigenvalue λ_n has multiplicity $2n + 1$. For the numerical approximation, we employ NURBS bases of degree $p = 2$ and C^1-continuous a.e. in Ω for $m = 2$, while for $m = 3$ we use NURBS bases of degree $p = 3$ and C^2-continuous a.e. in Ω. In Figure 11 we report the normalized spectra, i.e. the relative error $\lambda_{n,h}/\lambda_n$ vs. the normalized eigenvalue number n/n_{bf}, considering two different mesh sizes h for both the bilaplacian and trilaplacian eigenvalue problems.

6 Phase Field Models on Closed Surfaces

We consider the numerical approximation of two phase field models: the fourth order Cahn-Hilliard equation and the sixth order crystal equation on closed surfaces.

6.1 The Cahn-Hilliard equation

Spinodal decomposition is the process of phase separation undergone by a quenched homogeneous fluid mixture [8] and the Cahn-Hilliard equation is a stiff, nonlinear, fourth order parabolic equation which describes such spinodal decomposition for a binary fluid [21, 27]. Let $\Omega \subset \mathbb{R}^3$ be an arbitrary surface domain, then the binary fluid mixture is contained in Ω and the concentration of one of its components is denoted by $u = u(x, t) : \Omega \times (0, T) \to \mathbb{R}$. The Cahn-Hilliard equation models the dissipation of the Ginzburg-Landau free energy Ψ within a mass conservative system [9]: $\Psi = \Psi_c + \Psi_s$, where Ψ_c refers to the chemical free energy (bulk energy) and Ψ_s is the surface free energy. The chemical free energy describes the immiscibility of the mixture's components and, as far as isothermal binary mixtures are concerned, it can be written as $\Psi_c(u) = \dfrac{1}{2\theta}\left(u\log(u) + (1-u)\log(1-u)\right) + u(1-u)$, where θ is the ratio between the critical and

the absolute temperatures [9]; in this paper, we set $\theta = 3/2$, for which Ψ_c assumes the form of a double well in the variable u; the minimization of the chemical free energy leads to the separation of the phases. The surface free energy describes the attractive long-range interactions between the molecules of the binary mixture [27] and reads $\Psi_s(u) = \frac{1}{2}\lambda\nabla_\Omega u \cdot \nabla_\Omega u$, where the differential operators are defined on the surface Ω and the parameter λ characterizes the interface thickness between the phases by a length scale proportional to $\sqrt{\lambda}$. The minimization of the surface free energy leads to the coarsening of the phases; in fact, solutions of the Cahn-Hilliard equation for which Ψ is minimum correspond to the solutions of the isoperimetric problem [42].

In order to minimize the free energy Ψ while maintaining the constraint of mass conservation, we exploit the H^{-1} gradient flow of Ψ on the surface Ω as in [20]. Therefore, assuming suitable boundary conditions, we write the Fréchet derivative of the free energy as $\dfrac{\delta\Psi}{\delta u} = \mu_u - \lambda\Delta_\Omega u$, where μ_u is the chemical potential, corresponding to $\mu_u := \dfrac{d\Psi}{du} = \dfrac{1}{2\theta}\log\left(\dfrac{u}{1-u}\right) + 1 - 2u$. If the surface Ω is closed, i.e. if $\partial\Omega \equiv \emptyset$, the H^{-1} gradient flow leads to the following problem:

$$\begin{cases} \dfrac{\partial u}{\partial t} = \nabla_\Omega \cdot \left(M_u \nabla_\Omega \left(\mu_u - \lambda\Delta_\Omega u\right)\right) & \text{in } \Omega \times (0,T)\,, \\ u(0) = u_0 & \text{in } \Omega \times \{0\}\,, \end{cases} \tag{6.1}$$

where $M_u = M_0 u\,(1-u)$ is the degenerate mobility [8]. The problem is then rewritten in dimensionless form [27] before being discretized:

$$\text{find } u(t) \in L^2(0,T;V) \cap H^1(0,T;L^2(\Omega)) : \quad \begin{cases} \displaystyle\int_\Omega \frac{\partial u}{\partial t}\, v\, d\Omega + a(u(t))(v) = 0 & \forall v \in V, t \in (0,T)\,, \\ u(0) = u_0 & \text{in } \Omega, \end{cases} \tag{6.2}$$

where $V = H^2(\Omega)$,

$$a(u)(v) := \int_\Omega (\mathbb{N}_1 M_u \nabla_\Omega \mu_u + \nabla_\Omega M_u \Delta_\Omega u) \cdot \nabla_\Omega v\, d\Omega + \int_\Omega M_u\, \Delta_\Omega u\, \Delta_\Omega v\, d\Omega, \tag{6.3}$$

the differential operators are now dimensionless, and $\mathbb{N}_1 = \dfrac{L_0^2}{\lambda}$ is a dimensionless parameter, with L_0, M_0 and $T_0 = \dfrac{L_0^4}{\lambda M_0}$ the characteristic length, mobility and time scale, respectively; u_0 is the initial condition.

We specifically consider problem (6.1) on a unit sphere in $\mathbb{R}^3$. The geometry is described exactly by NURBS using a single patch. In order to approximate the solution, we consider a spatial discretization of the domain by means of NURBS-based IGA in the framework of the Galerkin method. Since the Cahn-Hilliard equation is a fourth order PDE, following the same approach outlined in Sections 2.2 and 4, we enforce at least global C^1-continuity of the NURBS basis functions on the sphere except at the poles. Finally, we rewrite problem (6.2) in the parametric domain $\widehat{\Omega}$, reading:

$$\text{find } \widehat{u}_h(t) \in L^2(0,T;\widehat{V}_h) \cap H^1(0,T;L^2(\widehat{\Omega})) : \quad \widehat{\text{Res}}(\widehat{u}_h(t))(\widehat{v}_h) = 0 \qquad \forall v_h \in \widehat{V}_h, t \in (0,T), \tag{6.4}$$

with the initial condition $\widehat{u}_h(0) = \widehat{u}_{h,0}$ in $\widehat{\Omega}$, $\widehat{V}_h := H^2(\widehat{\Omega}) \cap \widehat{\mathcal{N}}_h^{per}$, and $\widehat{\text{Res}}$ the weak residual defined as:

$$\widehat{\text{Res}}(\widehat{u}_h(t))(\widehat{v}_h) := \int_{\widehat{\Omega}} \frac{\partial \widehat{u}_h}{\partial t}\, \widehat{v}_h\, d\widehat{\Omega} + \widehat{a}(\widehat{u}_h(t))(\widehat{v}_h), \tag{6.5}$$

with $\widehat{a}(\cdot,\cdot)$ obtained by a pull-back operation on the form (6.3) and $\widehat{u}_{h,0}$ the pull-back of the L^2-projection of u_0 onto $\mathcal{N}_h$. The weak residual in Ω reads:

$$\text{Res}(u_h(t))(v_h) := \int_\Omega \frac{\partial u_h}{\partial t}\, v_h \, d\Omega + a(u_h(t))(v_h). \tag{6.6}$$

6.2 The phase field crystal equation

Materials are often characterized by the properties of their structure at the micro-scale level, which defines their behavior at macro-scales and, usually, their traits depend on topological defects at atomic length scale. In order to account for their complex structure, most material characterizations are based on discrete Molecular Dynamics models, which are accurate but subject to severe computational time constraints, since dealing with atomic scales and phonon time scales [22]. Continuum models, on the contrary, are able to cope with larger systems and longer time lengths, but with a loss in accuracy of the physical description. The phase field crystal equation [18, 19, 32, 22] is a recently developed model for the study of crystal growth in a pure supercooled liquid, for epitaxial growth, and for crack propagation in ductile materials. The model describes a two phase system at atomic length scales, thus embedding the physical properties of the microstructure in a diffusive time scale. The phase field crystal equation is based on the definition of a free energy functional, which is minimized by a periodic density field. In this way, the free energy functional "embeds" the periodicity nature of crystal structures directly into its formulation and naturally includes the elastic energy and symmetry properties of the periodic crystal field [18]. The solution of the crystal equation is then obtained by the minimization of the energy functional, under the constraint of mass preservation.

Let us consider a surface $\Omega \subset \mathbb{R}^3$ and the variable $u = u(x,t) : \Omega \times (0,T) \to \mathbb{R}$ as the local atomistic density describing the two-phase system. The liquid phase is characterized by spatially uniform values of u, while the crystal solid phase zone presents the typical symmetric and periodic structures of the crystal lattice. The free energy functional $\mathcal{C}$ describing the two-phase system reads [22]:

$$\mathcal{C}(u) := \int_\Omega \left(\Phi(u) + \frac{D}{2}k^4u^2 - Dk^2|\nabla_\Omega u|^2 + \frac{D}{2}(\Delta_\Omega u)^2 \right) d\Omega, \tag{6.7}$$

where D and k are positive constants and Φ is defined as $\Phi(u) := -\frac{\varepsilon}{2}u^2 - \frac{g}{3}u^3 + \frac{1}{4}u^4$, where ε and g are positive physical parameters. In order to minimize the free energy $\mathcal{C}$, we consider its Fréchet derivative obtained under suitable boundary conditions:

$$\frac{\delta \mathcal{C}(u)}{\delta u} = \phi(u) + Dk^4u + 2Dk^2\Delta_\Omega u + D\Delta_\Omega^2 u, \tag{6.8}$$

where $\phi(u) := \Phi'(u) = -\varepsilon u - gu^2 + u^3$. The evolution of u can then be described as the H^{-1} gradient flow of $\mathcal{C}$. By considering fully closed surfaces, we obtain the following nonlinear time-dependent sixth order PDE on the surface Ω:

$$\begin{cases} \dfrac{\partial u}{\partial t} = \Delta_\Omega \left(\phi(u) + Dk^4u + 2Dk^2\Delta_\Omega u + D\Delta_\Omega^2 u \right) & \text{in } \Omega \times (0,T)\,, \\ u(0) = u_0 & \text{in } \Omega \times \{0\}\,. \end{cases} \tag{6.9}$$

Problem (6.9) is conveniently rewritten in dimensionless form, for which its weak formulation reads:

$$\text{find } u(t) \in L^2(0,T;V) \cap H^1(0,T;L^2(\Omega)): \quad \begin{cases} \displaystyle\int_\Omega \frac{\partial u}{\partial t}\, v\, d\Omega + a(u(t))(v) = 0 & \forall v \in V, t \in (0,T), \\ u(0) = u_0 & \text{in } \Omega \times \{0\}, \end{cases} \tag{6.10}$$

where $V = H^3(\Omega)$,

$$\begin{aligned} a(u)(v) := & \int_\Omega \left(\phi'(u) + \mathbb{N}_1\right) \nabla_\Omega u \cdot \nabla_\Omega v \, d\Omega \\ & - \mathbb{N}_2 \int_\Omega \Delta_\Omega u \, \Delta_\Omega v \, d\Omega + \mathbb{N}_3 \int_\Omega \nabla_\Omega \left(\Delta_\Omega u\right) \cdot \nabla_\Omega \left(\Delta_\Omega v\right) \, d\Omega, \end{aligned} \tag{6.11}$$

the differential operators are now dimensionless, and $\mathbb{N}_1$, $\mathbb{N}_2$, and $\mathbb{N}_3$ are dimensionless parameters set as $\mathbb{N}_1 := \dfrac{Dk^4}{\phi_0}$, $\mathbb{N}_2 := \dfrac{2Dk^2}{\phi_0 L_0^2}$, and $\mathbb{N}_3 := \dfrac{D}{\phi_0 L_0^4}$, where L_0, ϕ_0 and $T_0 = \dfrac{L_0^2}{\phi_0}$ are characteristic values for length, Φ, and time.

We consider the approximation of problem (6.9) on a closed surface in $\mathbb{R}^3$, specifically a torus. The geometry is represented exactly by NURBS with a single patch and, as the previous example, we employ a spatial discretization by means of NURBS-based Galerkin IGA. Problem (6.9) is characterized by a sixth order PDE; therefore, the space $V \subseteq H^3(\Omega)$ and we employ NURBS bases of degree $p = 3$ for both representing the geometry and approximating the solution, the latter being globally C^2-continuous. Finally, problem (6.10) is rewritten in the parametric domain $\widehat{\Omega}$, obtaining the following semi-discretized problem:

$$\text{find } \widehat{u}_h(t) \in L^2(0,T;\widehat{V}_h) \cap H^1(0,T;L^2(\widehat{\Omega})): \quad \begin{cases} \widehat{\text{Res}}(\widehat{u}_h(t))(\widehat{v}_h) = 0 & \forall \widehat{v}_h \in \widehat{V}_h, t \in (0,T), \\ \widehat{u}_h(0) = \widehat{u}_{h,0} & \text{in } \widehat{\Omega} \times \{0\}, \end{cases} \tag{6.12}$$

where $\widehat{V}_h := H^3(\widehat{\Omega}) \cap \widehat{\mathcal{N}}_h^{per}$ and $\widehat{\text{Res}}$ is obtained performing the pull-back operation on the weak residual $\text{Res}(u_h(t))(v_h) := \displaystyle\int_\Omega \frac{\partial u_h}{\partial t}\, v_h \, d\Omega + a(u_h(t))(v_h)$.

6.3 Time discretization

As far as the time discretization is concerned, we employ for both the problems of Sections 6.1 and 6.2 the generalized-α method [10, 21, 27]. This is a fully implicit time integration scheme, with control on the numerical dissipation. Let us consider the approximated solution $\widehat{u}_h(t_n) = \widehat{u}_h^n$ at time t_n and discretized by means of NURBS-based IGA, such that:

$$\widehat{u}_h^n = \sum_{i=1}^{n_{bf}} \widehat{R}_i U_i(t_n) \qquad \text{and} \qquad \dot{\widehat{u}}_h^n = \sum_{i=1}^{n_{bf}} \widehat{R}_i \dot{U}_i(t_n), \tag{6.13}$$

the latter being the time derivative. Let us denote with $\mathbf{U}^n$ and $\dot{\mathbf{U}}^n$ the vectors of control variables associated with the solution and their time derivatives at time t_n, i.e. $\mathbf{U}^n = \{U_i(t_n)\}_{i=1}^{n_bf}$ and $\dot{\mathbf{U}}^n = \{\dot{U}_i(t_n)\}_{i=1}^{n_bf}$. By denoting the time step size by $\Delta t_n = t_{n+1} - t_n$, the generalized-$\alpha$ method applied to problems (6.4) and (6.12) consists in solving, at each time step t_n, with $n \geq 0$, the

following system of equations:

$$\begin{cases} \widehat{\mathbf{Res}}(\dot{\mathbf{U}}^{n+\alpha_m}, \mathbf{U}^{n+\alpha_f}) = 0 \\ \mathbf{U}^{n+\alpha_f} = \mathbf{U}^n + \alpha_f \left(\mathbf{U}^{n+1} - \mathbf{U}^n\right) \\ \dot{\mathbf{U}}^{n+\alpha_m} = \dot{\mathbf{U}}^n + \alpha_m \left(\dot{\mathbf{U}}^{n+1} - \dot{\mathbf{U}}^n\right) \\ \mathbf{U}^{n+1} = \mathbf{U}^n + \Delta t_n \dot{\mathbf{U}}^n + \delta \Delta t_n \left(\dot{\mathbf{U}}^{n+1} - \dot{\mathbf{U}}^n\right), \end{cases} \tag{6.14}$$

where the residual vector $\widehat{\mathbf{Res}}(\cdot,\cdot)$ is associated with the weak residuals in Eqs. (6.4) and (6.12). The parameters α_m, α_f and δ are chosen such that $\delta = \frac{1}{2} + \alpha_m - \alpha_f$ and $\alpha_m \geq \alpha_f \geq \frac{1}{2}$, leading to an unconditionally stable and second-order accurate method when employed for linear problems [26]. Moreover, they can be tuned to control the numerical dissipation of the high frequencies. By denoting with $\rho_\infty \in [0,1]$ the limit of the spectral radius of the amplification matrix for $\Delta t \to \infty$, the parameters can be chosen as $\alpha_m = \frac{1}{2}\left(\frac{3-\rho_\infty}{1+\rho_\infty}\right)$, $\alpha_f = \frac{1}{1+\rho_\infty}$, and $\delta = \frac{1}{1+\rho_\infty}$.

In order to solve the non-linear system of equations (6.14) resulting from time and space discretizations, we employ the Newton method [34]. Following [27], by denoting with the subscript k the current Newton iterate and with k_{max} the maximum number of sub-iterations allowed, this leads to the following predictor-multicorrector scheme at the discrete time steps t_n, with $n \geq 0$:

Predictor (initialization phase of Newton method):

$$\mathbf{U}_0^{n+1} = \mathbf{U}^n \quad \text{and} \quad \dot{\mathbf{U}}_0^{n+1} = \frac{\delta - 1}{\delta}\dot{\mathbf{U}}^n \tag{6.15}$$

Corrector: for $k = 0, \ldots, k_{max} - 1$

$$\dot{\mathbf{U}}_{k+1}^{n+\alpha_m} = \dot{\mathbf{U}}^n + \alpha_m \left(\dot{\mathbf{U}}_k^{n+1} - \dot{\mathbf{U}}^n\right) \quad \text{and} \quad \mathbf{U}_{k+1}^{n+\alpha_f} = \mathbf{U}^n + \alpha_f \left(\mathbf{U}_k^{n+1} - \mathbf{U}^n\right) \tag{6.16}$$

$$\mathbf{Q}_{k+1} := \mathbf{Res}\left(\dot{\mathbf{U}}_{k+1}^{n+\alpha_m}, \mathbf{U}_{k+1}^{n+\alpha_f}\right) \tag{6.17}$$

$$\mathbf{K}_{k+1} := \alpha_m \frac{\partial \mathbf{Res}\left(\dot{\mathbf{U}}_{k+1}^{n+\alpha_m}, \mathbf{U}_{k+1}^{n+\alpha_f}\right)}{\partial \dot{\mathbf{U}}^{n+\alpha_m}} + \alpha_f \delta \Delta t_n \frac{\partial \mathbf{Res}\left(\dot{\mathbf{U}}_{k+1}^{n+\alpha_m}, \mathbf{U}_{k+1}^{n+\alpha_f}\right)}{\partial \mathbf{U}^{n+\alpha_f}} \tag{6.18}$$

$$\text{solve } \mathbf{K}_{k+1} \Delta \dot{\mathbf{U}}_{k+1}^{n+1} = -\mathbf{Q}_{k+1} \tag{6.19}$$

$$\dot{\mathbf{U}}_{k+1}^{n+1} = \dot{\mathbf{U}}_k^{n+1} + \Delta \dot{\mathbf{U}}_{k+1}^{n+1} \quad \text{and} \quad \mathbf{U}_{k+1}^{n+1} = \mathbf{U}_k^{n+1} + \delta \Delta t_n \Delta \dot{\mathbf{U}}_{k+1}^{n+1}. \tag{6.20}$$

The corrector phase is executed until the relative norm of the residual $\frac{\|\mathbf{Q}_{k+1}\|}{\|\mathbf{Q}_0\|}$ is below a certain tolerance, or the maximum number of sub-iterations k_{max} is reached.

For the tests under consideration in Sections 6.4 and 6.5 we set $\rho_\infty = 0.5$ and the solution of the linear system (6.19) is performed with the GMRES method [37], with incomplete-LU factorization as preconditioner.

6.4 Test 4. Numerical results for the Cahn-Hilliard equation

Solutions of the Cahn-Hilliard equation are characterized by extremely different time scales. In order to obtain simulations reaching the steady state in reasonable computational times, it is

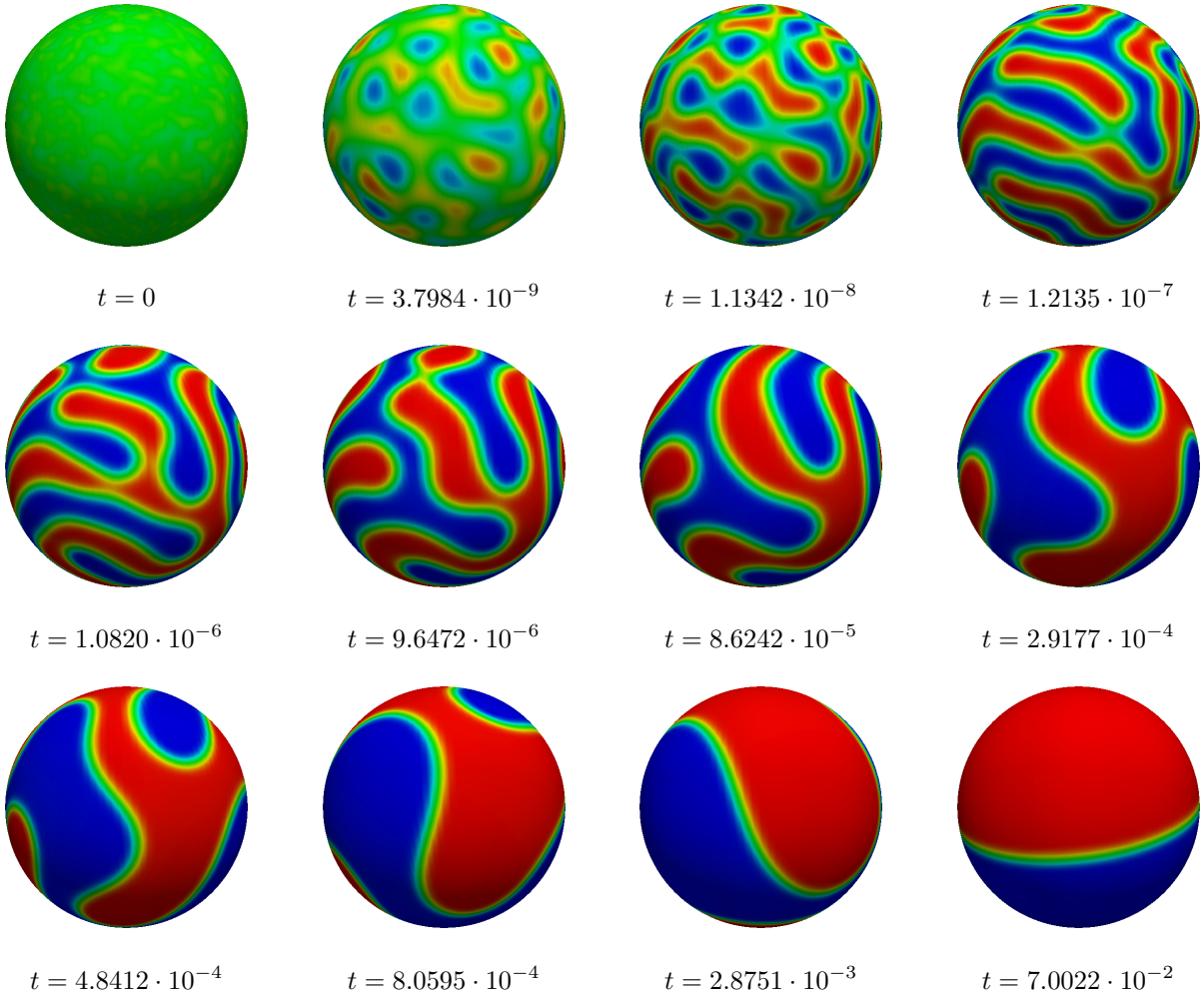

Figure 12: Test 4.1. Cahn-Hilliard equation on the sphere: evolution of the solution with volume fraction $v_f = 0.5$.

necessary to employ an adaptive time stepping procedure. We resort to the scheme proposed in [12, 21, 27], for which the adaptive scheme consists in solving the problem firstly with the generalized-α method and then with the Backward Euler method; then, the solution $\mathbf{U}_{\alpha}^{n+1}$ computed with the generalized-α method and the solution $\mathbf{U}_{BE}^{n+1}$ obtained with the Backward Euler method are compared using a suitable criterion and the time step size updated accordingly. Specifically, by denoting with i the iterate of the adaptive time stepping scheme, for $i = 0, \dots, i_{max}$ the solutions $\mathbf{U}_{\alpha,i}^{n+1}$ and $\mathbf{U}_{BE,i}^{n+1}$ are calculated with time step size $\Delta t_{n,i}$, having set $\Delta t_{n,0} = \Delta t_{n-1}$; then, based on the relative error $e_{n+1,i} := \dfrac{\|\mathbf{U}_{\alpha,i}^{n+1} - \mathbf{U}_{BE,i}^{n+1}\|}{\|\mathbf{U}_{\alpha,i}^{n+1}\|}$, the new time step size is computed as:

$$\Delta t_{n,i+1} = \gamma \sqrt{\frac{\tau}{e_{n+1,i}}} \Delta t_{n,i}, \tag{6.21}$$

where τ is a tolerance and γ a safety parameter. The adaptation loop continues until the error meets the tolerance τ or the maximum number of iterations i_{max} is reached. In this work, we set $\tau = 10^{-3}$ and $\gamma = 0.85$.

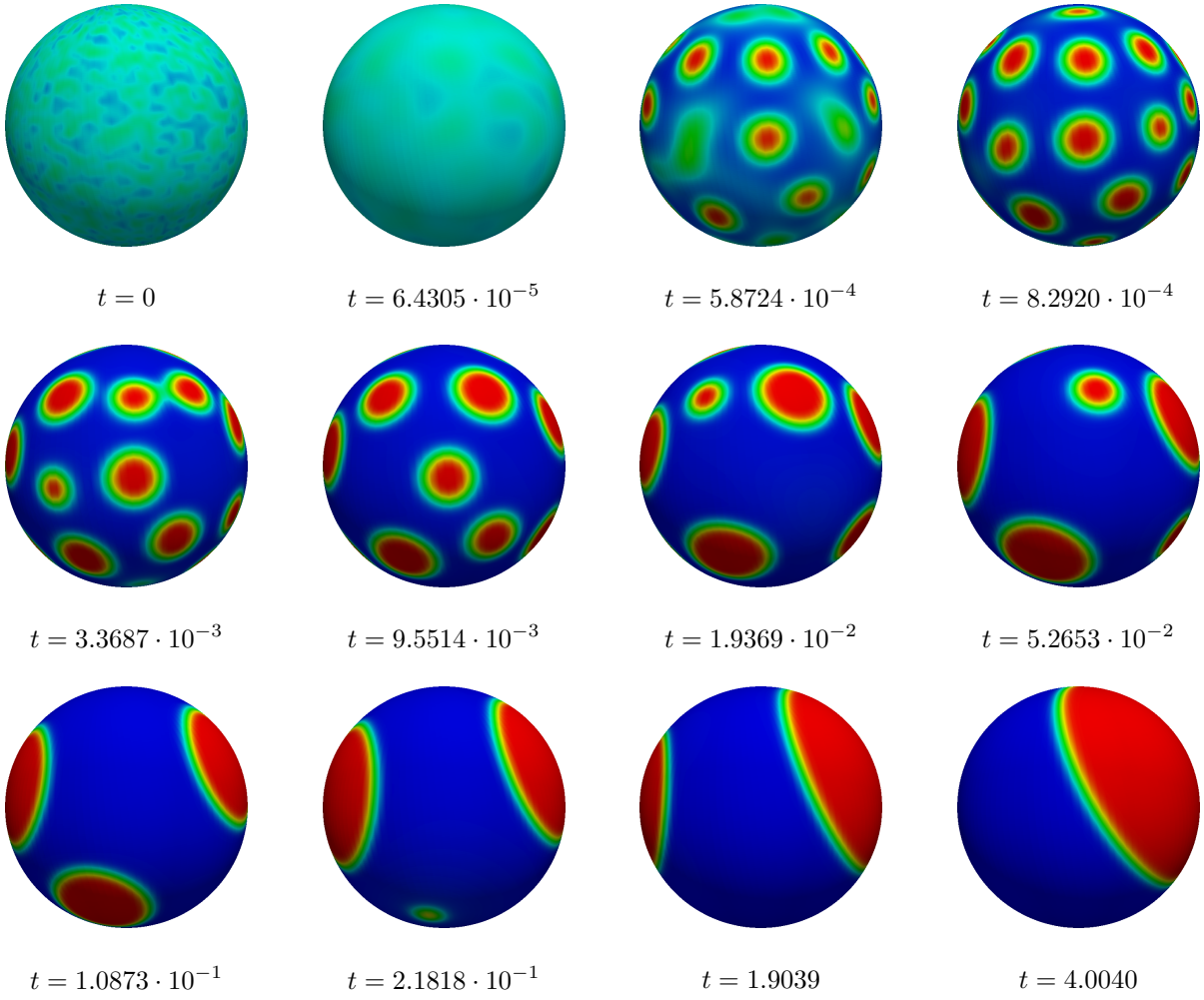

Figure 13: Test 4.2. Cahn-Hilliard equation on the sphere: evolution of the solution with volume fraction $v_f = 0.3$.

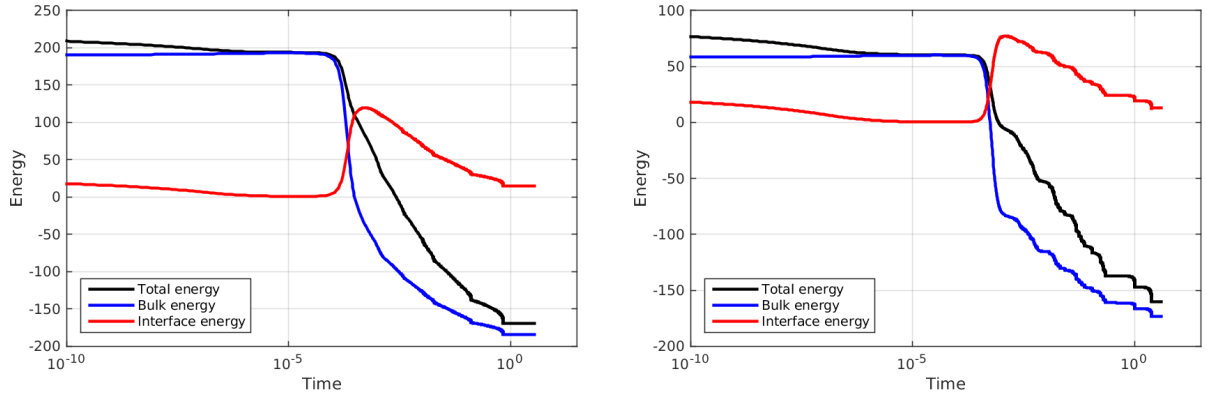

(a) $v_f = 0.5$ (Test 4.1) (b) $v_f = 0.3$ (Test 4.2)

Figure 14: Test 4. Cahn-Hilliard equation on the sphere: energies $\Psi(t)$, $\Psi_c(t)$, and $\Psi_s(t)$ vs. time, with volume fractions $v_f = 0.5$ (Test 4.1, left) and $v_f = 0.3$ (Test 4.2, right).

We consider two tests (Test 4.1 and 4.2) for which the initial data u_0 is built as a random mix of the phases. By denoting with $v_f = \dfrac{\int_\Omega u_0 \, d\Omega}{|\Omega|}$ the *volume fraction*, in Test 4.1 we set $v_f = 0.5$, while in Test 4.2 $v_f = 0.3$. For both tests we set $M_0 = 1$, $\lambda = 1.3144 \cdot 10^{-3}$, $L_0 = 1$ and we consider the spatial IGA approximation based on NURBS bases of degree $p = 2$ and C^1-continuous a.e. on Ω; the mesh is comprised of 8,844 elements for a total number of DOFs equal to 8,192. We initially set $\Delta t_0 = 10^{-14}$. The results are reported in Figure 12 (for Test 4.1) and Figure 13 (for Test 4.2), where we highlight the phase transition from the initial mixed condition to the steady state. The evolution of the total free energy $\Psi(t) = \Psi(u(t))$, as well as the chemical (bulk) $\Psi_c(t)$ and the surface $\Psi_s(t)$ energies, are reported in Figure 14.

6.5 Test 5. Numerical results for the phase field crystal equation

Unlike the Cahn-Hilliard equation, the phase field crystal equation does not involve large variations of the time scales; nevertheless, an adhoc and rapid time step size adaptivity scheme has been employed, in order to reduce the overall computational cost of the simulation: at each time step the successive time step size is calculated as the actual one rescaled by a factor depending on the number of Newton sub-iterations N_{newton} carried at the corrector stage of the generalized-α method. Specifically, $\Delta t_{n+1} = \min\{\beta_n \Delta t_n, \Delta t_{max}\}$, where:

$$\beta_n = \begin{cases} 1.2 & \text{if } N_{newton} < 3, \\ 1.1 & \text{if } N_{newton} = 3, \\ 0.8 & \text{if } N_{newton} = 4, \\ 0.5 & \text{if } N_{newton} > 4. \end{cases} \tag{6.22}$$

This is meant to keep the number of Newton sub-iterations between 3 and 4 at each time step, which seems to be a good compromise between the computational cost and the accuracy of the solution; moreover, with respect to the adaptivity scheme described in Section 6.4, it does not require the solution of two linear systems at each time step.

We consider the approximation of the phase field crystal equation on a torus (Test 5), with initial condition u_0 representing a single crystal immersed in a uniform liquid field. We choose the parameters $D = 10^6$, $k = 10^{-3/2}$, $L_0 = 1$, $\phi_0 = 5$, $g = 0$, and $\varepsilon = 1$, for which the dimensionless parameters are $\mathbb{N}_1 = 0.2$, $\mathbb{N}_2 = 4{\cdot}10^{-3}$, and $\mathbb{N}_3 = 2{\cdot}10^{-5}$, and the initial time step size $\Delta t_0 = 5{\cdot}10^{-5}$. We consider the spatial IGA approximation of problem (6.9) using NURBS basis functions of degree $p = 3$ and globally C^2-continuous on Ω; the mesh is comprised of 36,305 elements, for a total of 32,768 DOFs. The results are reported in Figure 15, while the evolution of the energy $\mathcal{C}(t)$ is reported in Figure 16, from which we observe that is monotonically decreasing in time.

7 Conclusions

In this work, we considered and discussed the numerical approximation of high order PDEs defined on surfaces by means of NURBS-based Isogeometric Analysis in the framework of the Galerkin method. We described the mathematical formulation of high order PDEs on surfaces, highlighting the benefits, with respect to the standard isoparametric FEM, of using NURBS function spaces for both spatially approximating the solution and representing the geometry according to the isogeometric concept; in particular, we detailed the role of the global continuity of the basis functions

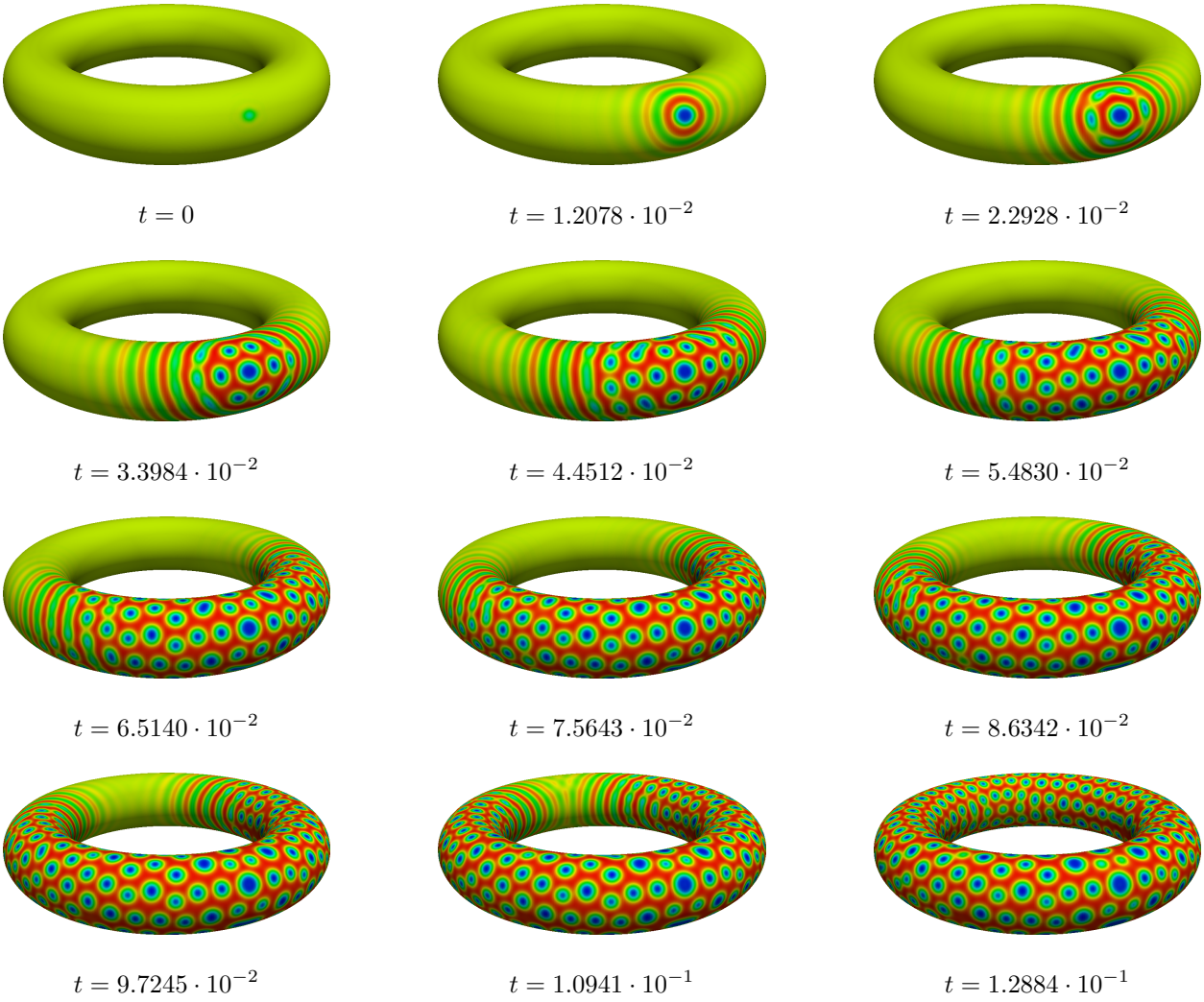

Figure 15: Test5. Phase field crystal equation on the torus: evolution of the solution.

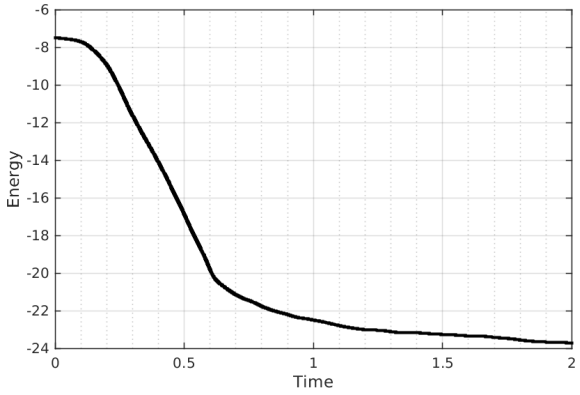

Figure 16: Test 5. Phase field crystal equation on the torus: energy $\mathcal{C}(t)$ vs. time.

in the physical domain for both open and closed single patch surfaces. We spatially approximated the fourth order Laplace-Beltrami biharmonic problem and the sixth order Laplace-Beltrami triharmonic problem on open and closed surfaces, with numerical results supporting the expected theoretical convergence rates; specifically, we considered the approximation of high order Laplace-Beltrami eigenvalue problems on the unit sphere. In general, the results showed that NURBS-based IGA is a very efficient tool when dealing with high order PDEs defined on surfaces and can be significantly more efficient than the isoparametric FEM applied to this class of problems. As further numerical validation, we considered phase field models which represent challenging time dependent, non linear, high order PDEs; specifically, we solved the fourth order Cahn-Hilliard equation on a sphere and the sixth order phase field crystal equation on a torus.

Acknowledgements

This work was partially supported by the Swiss National Science Foundation through the project "Isogeometric Analysis for Partial Differential Equations: surface models and optimization problems in Haemodynamics" (project ♯ 147,033). The authors acknowledge Prof. Fabio Nobile for fruitful discussions.

References

[1] R. A. Adams and J. J. F. Fournier. *Sobolev Spaces*, volume 140. Academic Press, 2003.

[2] M. Astorino, J. Hamers, S. C. Shadden, and J.-F. Gerbeau. A robust and efficient valve model based on resistive immersed surfaces. *International Journal for Numerical Methods in Biomedical Engineering*, 28(9):937–959, 2012.

[3] Y. Bazilevs, V. M. Calo, J. A. Cottrell, J. A. Evans, T. J. R. Hughes, S. Lipton, M. A. Scott, and T. W. Sederberg. Isogeometric Analysis using T–splines. *Computer Methods in Applied Mechanics and Engineering*, 199(5):229–263, 2010.

[4] M. Berger. *A Panoramic View of Riemannian Geometry*. Springer-Verlag, Berlin and Heidelberg, 2003.

[5] M. Bertalmıo, L.-T. Cheng, S. Osher, and G. Sapiro. Variational problems and partial differential equations on implicit surfaces. *Journal of Computational Physics*, 174(2):759–780, 2001.

[6] A. Bonito, R. H. Nochetto, and M. S. Pauletti. Geometrically consistent mesh modification. *SIAM Journal on Numerical Analysis*, 48(5):1877–1899, 2010.

[7] A. Bonito, R. H. Nochetto, and M. S. Pauletti. Dynamics of biomembranes: effect of the bulk fluid. *Mathematical Modelling of natural phenomena*, 6(05):25–43, 2011.

[8] J. W. Cahn. On spinodal decomposition. *Acta Metallurgica*, 9(9):795–801, 1961.

[9] J. W. Cahn and J. E. Hilliard. Free energy of a nonuniform system. I. Interfacial free energy. *The Journal of Chemical Physics*, 28(2):258–267, 1958.

[10] J. Chung and G. M. Hulbert. A time integration algorithm for structural dynamics with improved numerical dissipation: the generalized-α method. *Journal of Applied Mechanics*, 60(2):371–375, 1993.

[11] J. A. Cottrell, T. J. R. Hughes, and Y. Bazilevs. *Isogeometric Analysis: Toward Integration of CAD and FEA*. John Wiley & Sons, 2009.

[12] L. Cueto-Felgueroso and J. Peraire. A time–adaptive finite volume method for the Cahn-Hilliard and Kuramoto-Sivashinsky equations. *Journal of Computational Physics*, 227(24):9985–10017, 2008.

[13] L. Dedè and A. Quarteroni. Isogeometric Analysis for second order Partial Differential Equations on surfaces. *Computer Methods in Applied Mechanics and Engineering*, 284:807–834, 2015.

[14] M. C. Delfour and J. P. Zolésio. *Shapes and Geometries: Metrics, Analysis, Differential Calculus, and Optimization*. SIAM, Philadelphia (PA), 2011.

[15] G. Dziuk. Finite Elements for the Beltrami operator on arbitrary surfaces. In *Partial Differential Equations and Calculus of Variations*, volume 1357 of *Lecture Notes in Mathematics*, pages 142–155. Springer-Verlag, Berlin and Heidelberg, 1988.

[16] G. Dziuk and C. M. Elliott. Surface finite elements for parabolic equations. *Journal of Computational Mathematics*, 25(4):385–407, 2007.

[17] G. Dziuk and C. M. Elliott. Eulerian finite element method for parabolic PDEs on implicit surfaces. *Interfaces and Free Boundaries*, 10(119-138):464, 2008.

[18] K. R. Elder and M. Grant. Modeling elastic and plastic deformations in nonequilibrium processing using phase field crystals. *Physical Review E*, 70(5):051605, 2004.

[19] K. R. Elder, M. Katakowski, M. Haataja, and M. Grant. Modeling elasticity in crystal growth. *Physical Review Letters*, 88(24):245701, 2002.

[20] P. C. Fife. Models for phase separation and their Mathematics. *Electronic Journal of Differential Equations*, 2000(48):1–26, 2000.

[21] H. Gómez, V. M. Calo, Y. Bazilevs, and T. J. R. Hughes. Isogeometric Analysis of the Cahn–Hilliard phase-field model. *Computer Methods in Applied Mechanics and Engineering*, 197(49):4333–4352, 2008.

[22] H. Gómez and X. Nogueira. An unconditionally energy-stable method for the phase field crystal equation. *Computer Methods in Applied Mechanics and Engineering*, 249:52–61, 2012.

[23] J. B. Greer, A. L. Bertozzi, and G. Sapiro. Fourth order Partial Differential Equations on general geometries. *Journal of Computational Physics*, 216(1):216–246, 2006.

[24] T. J. R. Hughes. *The Finite Element Method: Linear Static and Dynamic Finite Element Analysis*. Dover Publications, Mineola, 2000.

[25] T. J. R. Hughes, J. A. Cottrell, and Y. Bazilevs. Isogeometric Analysis: CAD, finite elements, NURBS, exact geometry and mesh refinement. *Computer Methods in Applied Mechanics and Engineering*, 194(39):4135–4195, 2005.

[26] K. E. Jansen, C. H. Whiting, and G. M. Hulbert. A generalized-α method for integrating the filtered Navier-Stokes equations with a stabilized finite element method. *Computer Methods in Applied Mechanics and Engineering*, 190(3):305–319, 2000.

[27] J. Liu, L. Dedè, J. A. Evans, M. J. Borden, and T. J. R. Hughes. Isogeometric Analysis of the advective Cahn–Hilliard equation: spinodal decomposition under shear flow. *Journal of Computational Physics*, 242:321–350, 2013.

[28] K. Mekchay, P. Morin, and R. Nochetto. AFEM for the Laplace–Beltrami operator on graphs: design and conditional contraction property. *Mathematics of Computation*, 80(274):625–648, 2011.

[29] P. Morin, R. H. Nochetto, M. S. Pauletti, and M. Verani. AFEM for shape optimization. *MOX Report, Politecnico di Milano*, 29, 2011.

[30] M. S. Pauletti. *Parametric AFEM for geometric evolution equation and coupled fluid-membrane interaction*. PhD thesis, University of Maryland, 2008.

[31] L. A. Piegl and W. Tiller. *The NURBS Book*. Springer-Verlag, Berlin, 1997.

[32] N. Provatas, J. A. Dantzig, B. Athreya, P. Chan, P. Stefanovic, N. Goldenfeld, and K. R. Elder. Using the phase–field crystal method in the multi–scale modeling of microstructure evolution. *Journal of the Minerals, Metals and Materials Society*, 59(7):83–90, 2007.

[33] A. Quarteroni. *Numerical Models for Differential Problems*. Springer, Milan, 2014.

[34] A. Quarteroni, R. Sacco, and F. Saleri. *Numerical Mathematics*. Springer-Verlag, Berlin and Heidelberg, 2007.

[35] A. Rätz and A. Voigt. PDE's on surfaces – a diffuse interface approach. *Communications in Mathematical Sciences*, 4(3):575–590, 2006.

[36] M. Reuter, F.-E. Wolter, M. Shenton, and M. Niethammer. Laplace–Beltrami eigenvalues and topological features of eigenfunctions for statistical shape analysis. *Computer-Aided Design*, 41(10):739–755, 2009.

[37] Y. Saad and M. H. Schultz. GMRES: A generalized minimal residual algorithm for solving nonsymmetric linear systems. *SIAM Journal on Scientific and Statistical Computing*, 7(3):856–869, 1986.

[38] M. A. Scott, X. Li, T. W. Sederberg, and T. J. R. Hughes. Local refinement of analysis-suitable T–splines. *Computer Methods in Applied Mechanics and Engineering*, 213:206–222, 2012.

[39] T. W. Sederberg, J. Zheng, A. Bakenov, and A. Nasri. T–splines and T–NURCCs. In *ACM transactions on graphics (TOG)*, volume 22:3, pages 477–484. ACM, 2003.

[40] A. Tagliabue, L. Dedè, and A. Quarteroni. Isogeometric Analysis and error estimates for high order partial differential equations in fluid dynamics. *Computers & Fluids*, 102:277–303, 2014.

[41] S. Timoshenko and S. Woinowsky-Krieger. *Theory of Plates and Shells*. McGraw–Hill, New York, 1959.

[42] O. Wodo and B. Ganapathysubramanian. Computationally efficient solution to the Cahn-Hilliard equation: adaptive implicit time schemes, mesh sensitivity analysis and the 3D isoperimetric problem. *Journal of Computational Physics*, 230(15):6037–6060, 2011.

Recent publications:

MATHEMATICS INSTITUTE OF COMPUTATIONAL SCIENCE AND ENGINEERING
Section of Mathematics
Ecole Polytechnique Fédérale
CH-1015 Lausanne

43.2014 PAOLA F. ANTONIETTI, ILARIO MAZZIERI, ALFIO QUARTERONI:
Improving seismic risk protection through mathemactical modeling

44.2014 LUCA DEDÈ, ALFIO QUARTERONI, SEHNGFENG ZHU:
Isogeometric analysis and proper orthogonal decomposition for parabolic problems

45.2014 ZVONIMIR BUJANOVIC, DANIEL KRESSNER:
A block algorithm for computing antitriangular factorizations of symmetric matrices

46.2014 ASSYR ABDULLE:
The role of numerical integration in numerical in numerical homogenization

47.2014 ANDREA MANZONI, STEFANO PAGANI, TONI LASSILA:
Accurate solution of Bayesian inverse uncertainty quantification problems using model and error reduction methods

48.2014 MARCO PICASSO:
From the free surface flow of a viscoelastic fluid towards the elastic deformation of a solid

49.2014 FABIO NOBILE, FRANCESCO TESEI:
A multi level Monte Carlo method with control variate for elliptic PDEs with log-normal coefficients

***

01.2015 PENG CHEN, ALFIO QUARTERONI, GIANLUIGI ROZZA:
Reduced order methods for uncertainty quantification problems

02.2015 FEDERICO NEGRI, ANDREA MANZONI, DAVID AMSALLEM:
Efficient model reduction of parametrized systems by matrix discrete empirical interpolation

03.2015 GIOVANNI MIGLIORATI, FABIO NOBILE, RAÚL TEMPONE:
Convergence estimate in probability and in expectation for discrete least squares with noisy evaluations at random points

04.2015 FABIO NOBILE, LORENZO TAMELLINI, FRANCESCO TESEI, RAÚL TEMPONE:
An adaptive sparse grid alorithm for elliptic PDEs with lognormal diffusion coefficent

05.2015 MICHAEL STEINLECHNER:
Riemannian optimization for high-dimensional tensor completion

06.2015 V. R. KOSTIĆ, A. MIEDLAR, LJ. CVETKOVIĆ:
An algorithm for computing minimal Geršgorin sets

07.2015 ANDREA BARTEZZAGHI, LUCA DEDÈ, ALFIO QUARTERONI:
Isogeometric analysis of high order partial differential equations on surfaces